

MULTI-WAVELENGTH OBSERVATIONS OF SUPERNOVA 2011ei: TIME-DEPENDENT CLASSIFICATION OF TYPE IIb AND Ib SUPERNOVAE AND IMPLICATIONS FOR THEIR PROGENITORS

DAN MILISAVLJEVIC¹, RAFFAELLA MARGUTTI¹, ALICIA M. SODERBERG¹, GIULIANO PIGNATA², LAURA CHOMIUK^{3,1}, ROBERT A. FESEN⁴, FILOMENA BUFANO², NATHAN E. SANDERS¹, JEROD T. PARRENT^{4,5}, STUART PARKER, TIMOTHY PICKERING^{6,7}, DAVID A. H. BUCKLEY^{6,7}, STEVEN M. CRAWFORD^{6,7}, AMANDA A. S. GULBIS^{6,7}, CHRISTIAN HETTLAGE^{6,7}, ERIC HOOPER⁸, KENNETH H. NORDSIECK⁸, DARRAGH O'DONOGHUE⁷, TIM-OLIVER HUSSER⁹, STEPHEN POTTER⁶, ALEXEI KNIAZEV^{6,7}, PAUL KOTZE^{6,7}, ENCARNI ROMERO-COLMENERO^{6,7}, PETRI VAISANEN^{6,7}, MARSHA WOLF⁸, NORBERT BARTEL¹⁰, MICHAEL F. BIETENHOLZ^{10,11}, CLAES FRANSSON¹², PAOLO MAZZALI¹³, ANDREAS BRUNTHALER^{14,3}, SAYAN CHAKRABORTI¹⁵, EMILY M. LEVESQUE¹⁶, ANDREW MACFADYEN¹⁷, COLIN DRESCHER, GREG BOCK, PETER MARPLES, JOSEPH P. ANDERSON¹⁸, STEFANO BENETTI¹⁹, DANIEL REICHART²⁰, AND KEVIN IVARSEN²⁰

Draft version July 11, 2012

ABSTRACT

We present X-ray, UV/optical, and radio observations of the stripped-envelope, core-collapse supernova (SN) 2011ei, one of the least luminous SNe IIb or Ib observed to date. Our observations begin with a discovery within ~ 1 day of explosion and span several months afterward. Early optical spectra exhibit broad, Type II-like hydrogen Balmer profiles that subside rapidly and are replaced by Type Ib-like He-rich features on the timescale of one week. High-cadence monitoring of this transition identifies an absorption feature around 6250 Å to be chiefly due to hydrogen, as opposed to C II, Ne I, or Si II. Similarities between this observed feature and several SNe Ib suggest that hydrogen absorption attributable to a high velocity ($\gtrsim 12,000$ km s⁻¹) H-rich shell is not rare in Type Ib events. Radio observations imply a shock velocity of $v \approx 0.13c$ and a progenitor star mass-loss rate of $\dot{M} \approx 1.4 \times 10^{-5} M_{\odot} \text{ yr}^{-1}$ (assuming wind velocity $v_w = 10^3$ km s⁻¹). This is consistent with independent constraints estimated from deep X-ray observations with *Swift*-XRT and *Chandra*. We find the multi-wavelength properties of SN 2011ei to be consistent with the explosion of a lower-mass ($3 - 4 M_{\odot}$), compact ($R_* \sim 1 \times 10^{11}$ cm), He core star. The star retained a thin hydrogen envelope at the time of outburst, and was embedded in an inhomogeneous circumstellar wind suggestive of modest episodic mass-loss. We conclude that SN 2011ei's rapid spectral metamorphosis calls attention to time-dependent classifications that bias estimates of explosion rates for a subset of Type IIb and Ib objects. Further, that important information about a progenitor star's evolutionary state and associated mass-loss in the days to years prior to SN outburst can be inferred from timely multi-wavelength observations.

Subject headings: supernovae: general — supernova: individual (SN 2011ei)

¹ Harvard-Smithsonian Center for Astrophysics, 60 Garden Street, Cambridge, MA, 02138. Electronic address: dmil-isav@cfa.harvard.edu

² Departamento de Ciencias Físicas, Universidad Andres Bello, Avda. Republica 252, Santiago, Chile

³ National Radio Astronomy Observatory, P.O. Box O, Socorro, NM 87801, USA

⁴ Department of Physics & Astronomy, Dartmouth College, 6127 Wilder Lab, Hanover, NH, 03755

⁵ Las Cumbres Observatory Global Telescope Network, Goleta, CA, US

⁶ South African Astronomical Observatory, PO Box 9, Observatory 7935, Cape Town, South Africa

⁷ Southern African Large Telescope, PO Box 9, Observatory 7935, Cape Town, South Africa

⁸ Department of Astronomy, University of Wisconsin, Madison, WI 53706, USA

⁹ Institut für Astrophysik, Georg-August-Universität, Friedrich-Hund-Platz 1, 37077 Göttingen, Germany

¹⁰ Department of Physics and Astronomy, York University, Toronto, Ontario M3J 1P3, Canada

¹¹ Hartebeesthoek Radio Observatory, P.O. Box 443, Krugersdorp, 1740, South Africa

¹² Department of Astronomy, The Oskar Klein Centre, Stockholm University, 106 91 Stockholm, Sweden

¹³ Max-Planck-Institut für Astrophysik, Karl-Schwarzschild-Strasse 1, 85748 Garching, Germany

¹⁴ Max-Planck-Institut für Radioastronomie, Auf dem Hügel 69, 53121 Bonn, Germany

¹⁵ Department of Astronomy and Astrophysics, Tata Institute

of Fundamental Research, 1 Homi Bhabha Road, Mumbai 400 005, India

¹⁶ CASA, Department of Astrophysical and Planetary Sciences, University of Colorado, 389-UCB, Boulder, CO 80309, USA

¹⁷ Department of Physics, New York University, 4 Washington Place, New York, NY 10003

¹⁸ Departamento de Astronomia, Universidad de Chile, Casilla 36-D, Santiago, Chile

¹⁹ INAF - Osservatorio Astronomico di Padova, Vicolo dell'Osservatorio 5, I-35122, Padova, Italy

²⁰ Department of Physics and Astronomy, University of North Carolina at Chapel Hill, Campus Box 3255, Chapel Hill, NC 27599-3255, USA

1. INTRODUCTION

Core-collapse supernovae (SNe) are traditionally defined by their spectroscopic properties in the optical (see Filippenko 1997 for review). SNe Type II show hydrogen lines at all epochs. SNe Type Ib do not show hydrogen lines, but do show conspicuous He features, and SNe Type Ic show neither H nor He. These classifications are thought to reflect compositional differences in the envelopes of the massive progenitor stars immediately prior to explosion. The envelopes of SNe Ib are H-deficient while those of SNe Ic are both H- and He-deficient.

However, exceptions and transitional subtypes exist that blur these formal classifications. Observations of SN 1987K (Filippenko 1988) showed a gradual transition in its optical spectra from Type II-like lines at photospheric epochs ($\lesssim 2$ months post-outburst) to Type Ib-like features at nebular epochs ($\gtrsim 5$ months). This remarkable spectroscopic evolution demonstrated the existence of an intermediary between the H-rich Type II and H-deficient Type Ib and Ic classes (hereafter Type Ibc). SN 1993J (Filippenko et al. 1993) was a well-studied additional example of this breeching of SN classifications and has come to be thought of as a prototype of SNe Type I Ib (Woosley et al. 1994). Like the SNe Ibc objects, SNe I Ib are believed to be massive stars but only partially stripped of their outer H-rich envelopes.

The entire class of SNe I Ib and Ibc are collectively known as “stripped-envelope” events (Clocchiatti et al. 1997). The degree of H and He envelope deficiency is believed to be the consequence of varying degrees of a SN progenitor star’s mass-loss. Potential mechanisms for mass-loss include steady winds (Puls et al. 2008), eruptive mass-loss episodes (Smith & Owocki 2006), or mass transfer due to Roche lobe overflow in a close binary system (Podsiadlowski et al. 1992). It is an open issue which of these processes dominate, and whether these processes occur in relatively high-mass single stars ($M \gtrsim 20 M_{\odot}$), from lower-mass progenitors ($M \gtrsim 10 M_{\odot}$), or a mixture of both.

The wide diversity in a small number of well-observed objects has complicated attempts at establishing firm connections between SN subtypes and their progenitor systems. This has been particularly the case for the inferred progenitors of SNe I Ib, which have been quite varied among a few nearby cases. For example, late-time spectroscopic and photometric observations of SN 1993J showed compelling evidence for a massive binary companion to the red supergiant progenitor star (Maund et al. 2004). However, pre-explosion imaging with the *Hubble Space Telescope* of SN 2008ax suggest that it most likely came from a more compact progenitor, such as a single massive Wolf-Rayet (WR) star or an interacting binary in a low-mass cluster (Crockett et al. 2008). Most recently, there has been considerable discourse about a yellow supergiant discovered in pre-explosion imaging at the location of SN 2011dh and its viability as a candidate progenitor (Maund et al. 2011; Van Dyk et al. 2011; Arcavi et al. 2011; Soderberg et al. 2011; Murphy et al. 2011; Georgy 2012).

From a statistical standpoint, the relatively high frequency of stripped-envelope SNe (~ 30 per cent of all core-collapse events by volume; Li et al. 2011) in combination with ongoing non-detections of progeni-

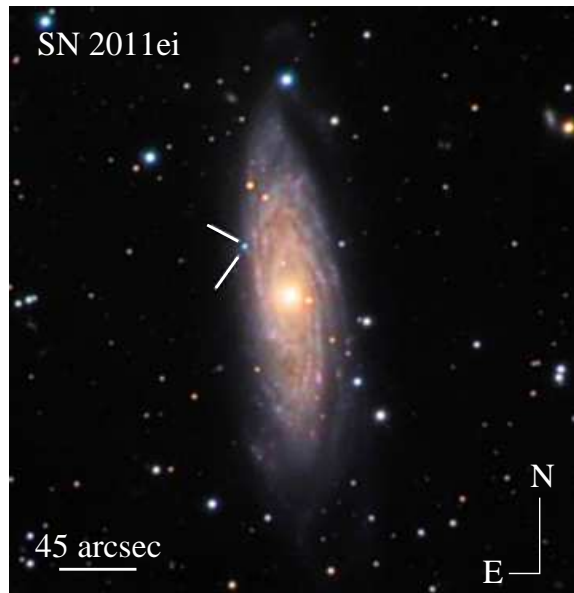


Figure 1. SN 2011ei around the time of maximum light in its host galaxy NGC 6925. This composite image was created from several exposures obtained with the 0.35-m telescope at Parkdale Observatory using *R*, *G*, *B*, *H α* , and clear filters.

tor stars in pre-explosion imaging (Smartt 2009) argues that at least some progenitor scenarios must involve massive stars in binary systems (Podsiadlowski et al. 1992; Fryer et al. 2007; Eldridge et al. 2008; Smith et al. 2011). Observational and theoretical investigations have suggested binary mass-loss scenarios that could lead to a spectroscopic sequence of SN types from I Ib \rightarrow Ib \rightarrow Ic (e.g., Filippenko et al. 1994; Woosley et al. 1994; Nomoto et al. 1995; Heger et al. 2003; Yoon et al. 2010; Dessart et al. 2011). Chevalier & Soderberg (2010) point out that the sequence may only be applicable for a subset of this population in light of optical and radio data that favor a division among SNe I Ib progenitors between objects like SN 1993J that have extended envelopes ($R_* \sim 10^{13}$ cm; referred to as Type “eI Ib”), and others like SN 2008ax that are more compact ($R_* \sim 10^{11}$ cm; Type “cI Ib”). They argue that Type cI Ib closely resemble Type Ib, and that the two subtypes may be related by a gradual transition depending on remaining H mass.

One key consequence of the proposed stripped-envelope sequence is that a thin hydrogen layer is expected to be present in many SNe Ib progenitors at the pre-supernova stage, and it is theorized that it may be possible to see hydrogen in their early spectra. Thus, the detection of hydrogen absorption lines at high velocity in SNe Ib is important because of its implications for the nature and evolutionary stage of the progenitor stars.

However, the presence of hydrogen observed in SNe Ib remains somewhat uncertain. Reports of suspected high-velocity ($\gtrsim 12,000$ km s $^{-1}$) hydrogen absorption around 6250 Å exist; e.g., SN 1999dn, SN 2000H (Branch et al. 2002); SN 2005bf (Anupama et al. 2005; Folatelli et al. 2006; Parrent et al. 2007), and SN 2008D (Soderberg et al. 2008). Alternative line identifications, however, have been offered. For instance, C II $\lambda 6580$, being less than 800 km s $^{-1}$ to the red of *H α* , has been considered a plausible identification (e.g., Harkness et al. 1987; Deng et al. 2000), and Si II $\lambda 6355$ and Ne I

Table 1
Combined *Swift*-UVOT and PROMPT photometry of SN 2011ei

| JD −2400000 | <i>uvw</i> 1 | <i>Swift</i> -UVOT | | <i>v</i> | <i>B</i> | PROMPT | | | |
|----------------|--------------|--------------------|------------|------------|--------------|--------------|--------------|--------------|-----|
| | | <i>u</i> | <i>b</i> | | | <i>V</i> | <i>R</i> | <i>I</i> | |
| 55769.73 | ... | ... | ... | ... | 19.264 0.058 | 18.786 0.104 | ... | ... | ... |
| 55770.65 | ... | ... | ... | ... | ... | 18.445 0.065 | 18.087 0.024 | 18.127 0.049 | ... |
| 55776.82 | ... | 16.67 0.06 | 17.63 0.07 | 17.58 0.11 | ... | ... | ... | ... | ... |
| 55776.84 | 17.95 0.07 | ... | ... | ... | ... | ... | ... | ... | ... |
| 55777.71 | 18.31 0.12 | 16.75 0.09 | 17.86 0.11 | ... | ... | ... | ... | ... | ... |
| 55778.52 | 17.90 0.13 | ... | ... | 17.53 0.21 | ... | ... | ... | ... | ... |
| 55779.25 | ... | 16.67 0.07 | 17.44 0.08 | ... | ... | ... | ... | ... | ... |
| 55779.32 | 17.82 0.09 | ... | ... | 17.41 0.15 | ... | ... | ... | ... | ... |
| 55780.64 | 17.91 0.10 | 16.61 0.08 | 17.38 0.08 | 17.31 0.14 | ... | ... | ... | ... | ... |
| 55782.61 | 17.90 0.10 | ... | ... | 17.10 0.12 | ... | ... | ... | ... | ... |
| 55783.14 | ... | 16.70 0.07 | 17.38 0.08 | ... | ... | ... | ... | ... | ... |
| 55783.75 | 18.04 0.16 | ... | ... | ... | ... | ... | ... | ... | ... |
| 55783.77 | ... | ... | ... | ... | 17.381 0.020 | 17.031 0.013 | 16.866 0.011 | 16.729 0.019 | ... |
| 55784.68 | ... | ... | ... | ... | 17.362 0.017 | 17.020 0.017 | 16.846 0.012 | 16.695 0.021 | ... |
| 55785.58 | ... | ... | ... | ... | 17.422 0.019 | 17.006 0.025 | 16.813 0.022 | ... | ... |
| 55788.13 | 18.31 0.11 | 17.27 0.10 | 17.48 0.09 | 16.99 0.11 | ... | ... | ... | ... | ... |
| 55788.70 | ... | ... | ... | ... | 17.636 0.018 | 17.006 0.019 | 16.796 0.013 | 16.575 0.021 | ... |
| 55788.96 | 18.40 0.12 | 17.44 0.11 | 17.48 0.09 | ... | ... | ... | ... | ... | ... |
| 55789.30 | ... | ... | ... | 17.07 0.10 | ... | ... | ... | ... | ... |
| 55789.66 | 18.56 0.13 | 17.55 0.12 | 17.49 0.09 | ... | ... | ... | ... | ... | ... |
| 55791.03 | 18.49 0.13 | 17.64 0.13 | 17.61 0.09 | ... | ... | ... | ... | ... | ... |
| 55791.44 | ... | ... | ... | 17.17 0.11 | ... | ... | ... | ... | ... |
| 55792.04 | 18.43 0.12 | ... | ... | ... | ... | ... | ... | ... | ... |
| 55792.23 | ... | 18.12 0.15 | 17.84 0.10 | ... | ... | ... | ... | ... | ... |
| 55792.63 | 18.74 0.23 | ... | ... | ... | ... | ... | ... | ... | ... |
| 55794.01 | 18.61 0.18 | ... | ... | ... | ... | ... | ... | ... | ... |
| 55794.48 | ... | 18.70 0.23 | 18.15 0.12 | ... | ... | ... | ... | ... | ... |
| 55794.59 | ... | ... | ... | ... | 18.345 0.031 | 17.354 0.019 | 16.950 0.019 | 16.626 0.026 | ... |
| 55795.18 | 18.93 0.16 | ... | ... | ... | ... | ... | ... | ... | ... |
| 55795.73 | ... | ... | ... | ... | 18.508 0.038 | 17.497 0.027 | 16.999 0.018 | 16.674 0.022 | ... |
| 55796.13 | ... | 19.12 0.29 | 18.41 0.15 | ... | ... | ... | ... | ... | ... |
| 55796.59 | 18.94 0.12 | ... | ... | ... | ... | ... | ... | ... | ... |
| 55798.09 | ... | ... | 18.61 0.16 | ... | ... | ... | ... | ... | ... |
| 55798.72 | ... | ... | ... | ... | 18.915 0.054 | 17.721 0.022 | 17.085 0.015 | 16.765 0.019 | ... |
| 55800.13 | 18.95 0.12 | 19.59 0.43 | ... | ... | ... | ... | ... | ... | ... |
| 55802.11 | ... | ... | 18.92 0.19 | ... | ... | ... | ... | ... | ... |
| 55802.74 | ... | ... | ... | ... | 19.131 0.242 | 17.980 0.034 | 17.210 0.017 | 16.846 0.018 | ... |
| 55804.04 | 19.04 0.12 | 20.05 0.63 | ... | ... | ... | ... | ... | ... | ... |
| 55805.77 | ... | ... | ... | ... | ... | 18.185 0.023 | 17.297 0.017 | 16.973 0.017 | ... |
| 55805.98 | ... | ... | 19.27 0.25 | ... | ... | ... | ... | ... | ... |
| 55808.15 | ... | 19.98 0.67 | ... | ... | ... | ... | ... | ... | ... |
| 55819.61 | ... | ... | ... | ... | ... | 18.337 0.055 | 17.552 0.020 | 17.167 0.024 | ... |

Note. — Uncertainties are adjacent to measurements and are at the 68% confidence level.

λ6402 have also been suggested (Hamuy et al. 2002; Tanaka et al. 2009; Branch 1972; Benetti et al. 2002).

The ambiguous identification of hydrogen in SNe Ib may be a consequence of current limitations in spectroscopic follow-up of SN candidates. Because spectra of SNe shortly after outburst are relatively rare, there is the possibility that SNe Iib vs. Ib (vs. Ic?) classification may be biased by the time of observation (see discussions by Branch et al. 2002 and Chornock et al. 2011). Indeed, precise rates of these events may be compromised by the dearth of early-time spectroscopic and photometric observations several days prior to maximum light when the SN is faint and the photosphere still resides in the outer layers of the progenitor star (Dessart et al. 2011). Almost half of the ejecta mass may have passed through the photosphere by the time peak brightness is reached, thus observations within a few days of explosion offer useful constraints on the progenitor star’s current evolutionary state (Yoon et al. 2010).

Our discovery and subsequent monitoring of SN 2011ei is an example of the utility of very early data. Discovered in NGC 6925 on July 25.434 UT (all future

dates also in UT; see Figure 1), early optical spectra of SN 2011ei initially showed line features similar to the Type Iib SN 1993J and SN 1996cb, but with a noticeably broader H-alpha P-Cygni profile reminiscent of the energetic Type Iib SN 2003bg (Stritzinger et al. 2011; Milisavljevic et al. 2011). However, spectra taken approximately one week later showed rapid evolution away from strong hydrogen features to conspicuous Type Ib-like helium absorptions.

This rapid change in SN 2011ei’s spectral properties along with a contemporaneous radio detection motivated a coordinated, multi-wavelength monitoring program presented here. In Section 2, 3, 4, and 5 we present and analyze X-ray, ultraviolet (UV), optical, and radio observations from *Swift*, *Chandra*, and ground-based observatories including the Southern African Large Telescope (SALT), Magellan, and the Karl G. Jansky Very Large Array (VLA). In Section 6 we discuss the implications these findings have for SN 2011ei’s progenitor star and its mass-loss history. Finally, in Section 7, we summarize our findings and discuss their relevance to a wider subset of stripped-envelope core-collapse SNe.

Table 2
PROMPT photometry of the local sequence stars in the field of NGC 6925

| No. | RA(J2000.0) | DEC(J2000.0) | <i>B</i> | <i>V</i> | <i>R</i> | <i>I</i> |
|-----|--------------|--------------|--------------|--------------|--------------|--------------|
| 1 | 20:34:31.425 | -31:55:37.13 | 15.350 0.023 | 14.658 0.033 | 14.268 0.036 | 13.898 0.081 |
| 2 | 20:34:28.104 | -31:55:54.40 | 17.904 0.031 | 17.183 0.027 | 16.758 0.025 | 16.380 0.025 |
| 3 | 20:34:26.771 | -31:57:32.56 | 15.680 0.015 | 14.989 0.027 | 14.574 0.037 | 14.220 0.048 |
| 4 | 20:34:37.298 | -31:59:10.83 | 16.843 0.012 | 16.105 0.034 | 15.666 0.044 | 15.235 0.048 |
| 5 | 20:34:35.922 | -31:59:48.73 | 17.746 0.023 | 17.335 0.031 | 17.027 0.045 | 16.724 0.046 |
| 6 | 20:34:37.883 | -32:00:03.00 | 17.721 0.028 | 17.053 0.031 | 16.660 0.017 | 16.283 0.029 |
| 7 | 20:34:35.853 | -32:00:08.29 | 17.139 0.057 | 16.464 0.039 | 16.041 0.028 | 15.682 0.062 |
| 8 | 20:34:35.118 | -32:00:55.90 | 17.349 0.029 | 16.411 0.024 | 15.858 0.048 | 15.404 0.064 |
| 9 | 20:34:32.157 | -32:01:06.60 | 17.927 0.011 | 17.396 0.035 | 17.065 0.033 | 16.720 0.046 |
| 10 | 20:34:32.166 | -32:01:22.16 | 17.658 0.062 | 17.061 0.052 | 16.690 0.040 | 16.344 0.046 |
| 11 | 20:34:32.923 | -32:01:43.05 | 18.444 0.020 | 17.061 0.018 | 16.129 0.046 | 15.359 0.078 |
| 12 | 20:34:33.090 | -32:02:17.52 | 17.200 0.054 | 16.363 0.034 | 15.877 0.045 | 15.429 0.063 |
| 13 | 20:34:31.201 | -32:02:05.58 | 18.535 0.158 | 17.278 0.037 | 16.383 0.062 | 15.722 0.063 |
| 14 | 20:34:31.086 | -32:03:03.46 | 18.073 0.053 | 17.483 0.039 | 17.105 0.054 | 16.738 0.024 |
| 15 | 20:34:25.617 | -32:02:06.45 | 17.324 0.052 | 16.661 0.033 | 16.249 0.049 | 15.902 0.072 |
| 16 | 20:34:26.544 | -32:00:29.45 | 17.576 0.026 | 16.749 0.036 | 16.264 0.046 | 15.835 0.073 |
| 17 | 20:34:24.061 | -32:00:48.81 | 16.666 0.045 | 15.924 0.044 | 15.477 0.046 | 15.094 0.064 |
| 18 | 20:34:23.184 | -32:01:34.76 | 18.284 0.047 | 17.222 0.044 | 16.590 0.033 | 16.110 0.072 |
| 19 | 20:34:19.306 | -32:02:19.59 | 15.962 0.029 | 15.272 0.038 | 14.852 0.050 | 14.492 0.070 |
| 20 | 20:34:18.786 | -32:01:26.81 | 18.255 0.012 | 17.336 0.064 | 16.765 0.069 | 16.343 0.033 |
| 21 | 20:34:14.755 | -32:03:33.72 | 18.784 1.180 | 17.378 0.044 | 16.967 0.047 | 16.621 0.085 |
| 22 | 20:34:12.242 | -32:03:10.87 | 16.758 0.043 | 15.789 0.024 | 15.227 0.051 | 14.758 0.075 |
| 23 | 20:34:08.874 | -32:02:50.79 | 15.787 0.016 | 14.658 0.029 | 13.920 0.051 | 13.372 0.080 |
| 24 | 20:34:00.474 | -32:02:38.43 | 17.707 0.053 | 16.833 0.041 | 16.307 0.035 | 15.873 0.079 |
| 25 | 20:33:57.672 | -32:01:02.46 | 16.610 0.053 | 15.841 0.033 | 15.367 0.051 | 14.979 0.088 |
| 26 | 20:34:01.183 | -32:00:02.73 | 16.535 0.057 | 15.962 0.035 | 15.593 0.046 | 15.264 0.070 |
| 27 | 20:34:00.268 | -31:58:22.97 | 17.099 0.028 | 16.428 0.030 | 16.014 0.051 | 15.648 0.062 |
| 28 | 20:34:01.183 | -32:00:02.74 | 16.535 0.057 | 15.962 0.035 | 15.593 0.046 | 15.264 0.070 |
| 29 | 20:34:00.266 | -31:58:22.97 | 17.099 0.028 | 16.428 0.030 | 16.014 0.051 | 15.648 0.062 |
| 30 | 20:34:08.158 | -31:57:16.48 | 16.710 0.011 | 15.213 0.029 | 14.229 0.049 | 13.177 0.067 |
| 31 | 20:33:59.155 | -31:57:09.43 | 16.886 0.037 | 15.662 0.026 | 14.842 0.022 | 14.274 0.077 |
| 32 | 20:34:08.192 | -31:56:53.97 | 17.899 0.011 | 17.300 0.013 | 16.881 0.010 | 16.549 0.054 |
| 33 | 20:34:07.231 | -31:56:43.23 | 17.737 0.026 | 17.125 0.043 | 16.745 0.036 | 16.382 0.052 |
| 34 | 20:34:06.013 | -31:55:43.34 | 15.450 0.034 | 14.718 0.032 | 14.296 0.043 | 13.918 0.080 |
| 35 | 20:34:10.459 | -31:55:13.60 | 15.872 0.028 | 15.244 0.045 | 14.878 0.044 | 14.508 0.062 |
| 36 | 20:34:17.120 | -31:56:23.58 | 17.916 0.102 | 17.413 0.060 | 17.027 0.051 | 16.678 0.035 |

Note. — Uncertainties are adjacent to measurements and are at the 68% confidence level.

2. OBSERVATIONS

2.1. Distance and Reddening

Located at coordinates $\alpha = 20^{\text{h}}34^{\text{m}}48^{\text{s}}.88$ and $\delta = -32^{\circ}58'23''.6$ (J2000.0), SN 2011ei is situated in projection along the outer periphery of its host spiral galaxy NGC 6925. Estimates of the distance to NGC 6925 via Tully-Fisher measurements range between 23.3 Mpc and 35.2 Mpc (Willick et al. 1997). For all calculations we adopt a distance $D \approx 28.5$ Mpc and a distance modulus $\mu = 32.27 \pm 0.43$ (Springob et al. 2009).

The reddening due to the Milky Way in the direction of NGC 6925 is $E(B - V)_{mw} = 0.059$ mag according to the infrared dust maps of Schlegel et al. (1998). NGC 6925 is highly inclined which would suggest possibly significant local extinction along its disk plane. The supernova, however, appears to lie on the galaxy's near side. We used the empirically derived relation between equivalent width (EW) and of Na I D absorption and $E(B - V)$ described in Turatto et al. (2003) to estimate the host extinction (though for a discussion of possible problems with this relationship, see, e.g., Poznanski et al. 2011). The $EW(\text{Na I D}) = 1.14 \pm 0.10$ Å absorption at the redshift of NGC 6925 determined from the weighted average of five spectra suggests an internal extinction of $E(B - V)_{\text{host}} = 0.18$ mag. Combining the inferred host and Galactic extinction, we adopt a total reddening $E(B - V) = 0.24$ mag and assume

$R_V = A_V/E(B - V) = 3.1$. However, in Section 3 we show that this estimate of the reddening is likely an upper limit.

2.2. X-ray Observations with *Swift*-XRT and *Chandra*

We promptly requested X-ray observations from the *Swift* spacecraft (Gehrels et al. 2004) using the XRT instrument (Burrows et al. 2005) beginning 2011 August 3.2. The total exposure time was 54 ks. Data were analyzed using the latest version of the HEASOFT package available at the time of writing (v. 6.11) and corresponding calibration files. Standard filtering and screening criteria were applied. No X-ray source is detected coincident with SN 2011ei with a 3 sigma upper limit of $4 \times 10^{-3} \text{ c s}^{-1}$ in the 0.3-10 keV band. The Galactic neutral hydrogen column density in the direction of SN 2011ei is $4.76 \times 10^{20} \text{ cm}^{-2}$ (Kalberla et al. 2005). Assuming a spectral photon index $\Gamma = 2$, this translates to an absorbed (unabsorbed) flux of $1.4 \times 10^{-13} \text{ erg cm}^{-2} \text{ s}^{-1}$ ($1.6 \times 10^{-13} \text{ erg cm}^{-2} \text{ s}^{-1}$), corresponding to a luminosity of $1.5 \times 10^{40} \text{ erg s}^{-1}$.

From the *Swift*-XRT images, X-ray contamination from the host galaxy nucleus is clearly identified at the SN site. Consequently, a 10 ks *Chandra* X-ray Observatory observation was also obtained on 2011 August 21 to resolve SN emission from the host galaxy nucleus (PI Soderberg, Prop. 12500613). Data were reduced with the CIAO software package (version 4.3) with calibra-

tion database CALDB (version 4.4.2). Standard filtering using CIAO threads for ACIS data were applied.

Consistent with the *Swift*-XRT observation, no X-ray source is detected at the SN position in the *Chandra* observation with a 3σ upper limit of $7.6 \times 10^{-4} \text{ c s}^{-1}$ in the 0.5–8 keV band. From the count-rate an absorbed flux limit of $5.5 \times 10^{-15} \text{ erg s}^{-1} \text{ cm}^{-2}$ is derived. Using the Galactic relations between N_{H} and A_V (Predehl & Schmitt 1995; Watson 2011), an intrinsic hydrogen column density $N_{\text{H}[\text{int}]} \sim 1.5 \times 10^{21} \text{ cm}^{-2}$ is inferred. Accounting for the total absorption (Galactic plus intrinsic) leads to a unabsorbed flux limit of $7 \times 10^{-15} \text{ erg s}^{-1} \text{ cm}^{-2}$ (assuming a simple power-law model with spectral photon index $\Gamma = 2$), corresponding to an X-ray luminosity of $L_{X[0.5-8\text{keV}]} < 7 \times 10^{38} \text{ erg s}^{-1}$. By comparison, X-ray emission at similar epochs from a SN IIb such as SN 1993J would have been detected ($L_{X[0.3-8\text{keV}]} \approx 8 \times 10^{39} \text{ erg s}^{-1}$), whereas the emission from an object like SN 2011dh ($L_{X[0.3-8\text{keV}]} \approx 1.5 \times 10^{38} \text{ erg s}^{-1}$) would not have been detected (Soderberg et al. 2011).

2.3. Ultraviolet and Optical Photometry

UV/optical observations of SN 2011ei with the *Swift*-UVOT instrument (Romig et al. 2005) began 2011 August 3.2 and continued through to 2011 September 10.9. Data were acquired using all of its six broad band filters that span the wavelength range of approximately 1600 – 6000 Å. The *Swift*-UVOT photometry presented in Table 1 is based on the photometric system described in Poole et al. (2008). In this system the *Swift* *b* and *v* filters are roughly equivalent to the standard Johnson Kron-Cousins *B* and *V* filters (see Poole et al. 2008 for details).

We analyzed the *Swift*-UVOT photometric data following the prescriptions of Brown et al. (2009). A $3''$ aperture was used to maximize the signal-to-noise (S/N) ratio. Late-time images acquired 2012 March 27 – April 6 have been used to estimate and remove the underlying host galaxy contribution. Observations beyond 2011 September 08 are not reported because supernova emission at these epochs was comparable to the underlying host galaxy. Also not reported are observations in the *uvw2* and *uvm2* filters where the SN was not detected with significant S/N.

Imaging in the Johnson Kron-Cousins *BVRI* filters was acquired with the Panchromatic Robotic Optical Monitoring and Polarimetry Telescope (PROMPT; Reichart et al. 2005) PROMPT3 and PROMPT5 located at Cerro Tololo Inter-American Observatory. All optical images were dark subtracted and flat-field corrected. Frames taken with the same filter were alienated and stacked in order to produce a final deeper image. The instrumental magnitude of the SN was measured in all the stacked frames using the PSF technique after being corrected for contaminating host emission via late-time template images. SN photometry was then calibrated against a sequence of stars located close to the SN. This local sequence, with magnitudes reported in Table 2, was calibrated to the standard Johnson Kron-Cousins photometric systems using observations of Landolt (1992, 2007) standard stars. The final magnitudes are reported in Table 1.

In addition to *Swift*-UVOT and PROMPT photometry, we estimate an apparent magnitude $R = 18.0 \pm 0.4$ on 2011 July 25.434 (JD 2455767.93) based on unfiltered discovery images of the SN. The data were obtained with the 0.35-m Celestron telescope equipped with a KAF-3200ME camera at Parkdale Observatory, Canterbury, New Zealand. After flat-fielding and correcting for the bias and dark current levels, SN emission was calibrated against field comparison stars of the USNO-B 1.0 star catalog and then converted to the standard Johnson Kron-Cousins *R* value.

2.4. Optical Spectroscopy

A total of 15 epochs of long slit optical spectra of SN 2011ei were collected. The details of all observations are provided in Table 3 and the reduced spectra are plotted in Figure 2. Most observations were made at SAAO Observatory with the 10-m Southern African Large Telescope (SALT) using the Robert Stobie Spectrograph (RSS; Burgh et al. 2003). The holographic grism pg0900 was used at combinations of four tilts to span a wavelength window of 3200 – 9000 Å and cover gaps between CCD detectors. On chip CCD 4×4 binning in the spectral and spatial directions was employed, yielding a dispersion of $1.96 \text{ Å pixel}^{-1}$ and $\approx 6 \text{ Å}$ full-width-at-half-maximum (FWHM) resolution. An atmospheric dispersion corrector minimized the effects of atmospheric refraction for all observations which were made generally around an airmass of 1.2. Conditions were mostly non-photometric with a median seeing around $1''.3$.

Additional spectra were obtained using a variety of telescopes and instrumental setups. Both the Magellan 6.5-m Baade and Clay telescopes located Las Campanas Observatory were used with the IMACS (Bigelow et al. 1998) and LDSS-3¹ instruments, respectively. The 3.6-m New Technology Telescope (NTT) located at La Silla was used with the EFOSC2² instrument, and the Southern Astrophysical Research (SOAR) 4.1-m telescope located at Cerro Pachón was used with the Goodman spectrograph (Clemens et al. 2004).

Reduction of all spectra followed standard procedures using the IRAF/PyRAF software. SALT data were first processed by the PySALT³ pipeline (see Crawford et al. 2010). Wavelength calibrations were made with arc lamps and verified with the night sky lines. Relative flux calibrations were made from observations of spectrophotometric standard stars from Oke (1990) and Hamuy et al. (1992, 1994). Gaps between CCD chips have been interpolated in instances when dithering between exposures was not possible, and cosmetic defects have been cleaned manually.

A recession velocity of 2780 km s^{-1} determined from coincident nebular H α emission has been removed from the presented spectra. This velocity is in agreement with a previous measurement of $2792 \pm 4 \text{ km s}^{-1}$ reported by Koribalski et al. (2004) using radio H I lines from the host NGC 6925.

2.5. Radio Observations with the VLA

¹ <http://www.lco.cl/telescopes-information/magellan/instruments-1/ldss-3-1/>

² <http://www.eso.org/sci/facilities/lasilla/instruments/efosc/>

³ <http://pysalt.salt.ac.za/>

Table 3
Summary of optical spectroscopic observations of SN 2011ei

| Date (UT) | JD −2400000 | Phase ^a (days) | Wavelength Range (Å) | Resolution ^b (Å) | Telescope/ Instrument | Exposure (s) |
|--------------|----------------|------------------------------|-------------------------|--------------------------------|--------------------------|-----------------|
| 2011 Jul 29 | 55772.32 | -14 | 3200 – 9000 | 6 | SALT/RSS | 2 × 300 |
| 2011 Aug 02 | 55776.33 | -10 | 3200 – 9000 | 6 | SALT/RSS | 2 × 300 |
| 2011 Aug 06 | 55780.31 | -6 | 3200 – 9000 | 6 | SALT/RSS | 2 × 600 |
| 2011 Aug 08 | 55782.30 | -4 | 3400 – 8800 | 6 | SALT/RSS | 1 × 600 |
| 2011 Aug 09 | 55783.30 | -3 | 5900 – 9000 | 6 | SALT/RSS | 1 × 600 |
| 2011 Aug 16 | 55789.54 | 3 | 3400 – 9000 | 6 | SALT/RSS | 2 × 600 |
| 2011 Aug 21 | 55794.62 | 8 | 3600 – 8900 | 13 | SOAR/Goodman | 3 × 450 |
| 2011 Aug 26 | 55799.50 | 13 | 3400 – 9000 | 6 | SALT/RSS | 1 × 600 |
| 2011 Aug 29 | 55803.48 | 17 | 3400 – 9000 | 6 | SALT/RSS | 1 × 600 |
| 2011 Sep 20 | 55824.43 | 38 | 3500 – 9500 | 4 | Magellan/IMACS | 1 × 900 |
| 2011 Sep 30 | 55834.63 | 48 | 3800 – 9400 | 6 | Magellan/LDSS3 | 3 × 900 |
| 2011 Oct 18 | 55852.55 | 66 | 3700 – 9200 | 18 | NTT/EFOSC2 | 2 × 1800 |
| 2011 Oct 24 | 55859.34 | 73 | 3400 – 8800 | 6 | SALT/RSS | 1 × 600 |
| 2011 Nov 16 | 55881.55 | 95 | 3800 – 8900 | 13 | SOAR/Goodman | 2 × 2700 |
| 2011 Nov 18 | 55883.55 | 97 | 3500 – 9500 | 4 | Magellan/IMACS | 1 × 1200 |

^a Phase is with respect to *V*-band maximum on JD 2455786.5 (2011 Aug 13.0).

^b FWHM of night sky emission lines.

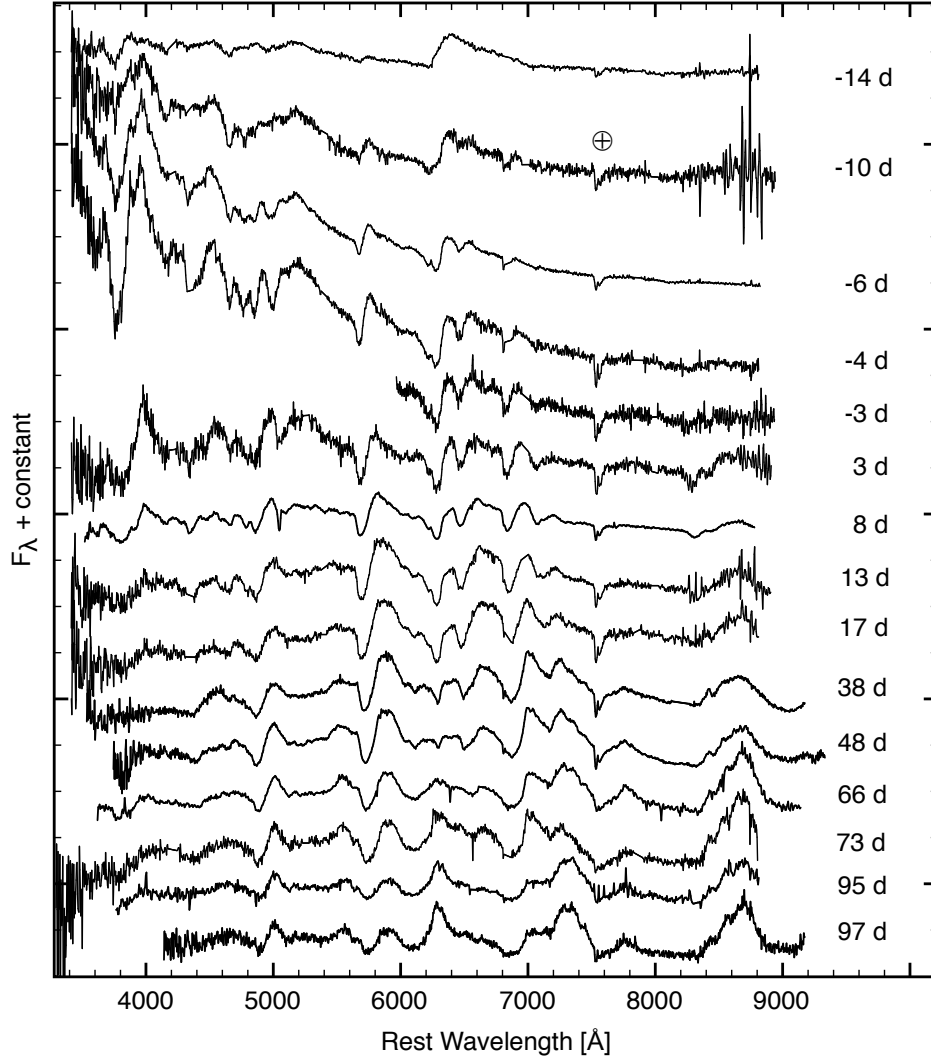


Figure 2. Optical spectra of SN 2011ei. Phase is with respect to *V*-band maximum. Telluric features have been marked with the “ \oplus ” symbol.

Table 4
VLA observations of SN 2011ei

| Date (UT) | ν (GHz) | F_ν (μ Jy) | Array Config. |
|---------------|-------------|---------------------|---------------|
| 2011 Aug 3.2 | 5.0 | 93 ± 25 | A |
| ... | 25 | 130 ± 140 | ... |
| 2011 Aug 5.2 | 5.0 | 143 ± 30 | A |
| 2011 Aug 7.2 | 3.1 | 37 ± 45 | A |
| ... | 5.0 | 226 ± 38 | ... |
| ... | 8.5 | 589 ± 38 | ... |
| 2011 Aug 12.2 | 3.1 | 143 ± 45 | A |
| ... | 5.0 | 289 ± 33 | ... |
| ... | 8.5 | 589 ± 38 | ... |
| 2011 Aug 17.3 | 3.1 | 289 ± 68 | A |
| ... | 5.0 | 564 ± 33 | ... |
| ... | 8.5 | 743 ± 38 | ... |
| 2011 Aug 25.2 | 3.1 | 353 ± 52 | A |
| ... | 5.0 | 511 ± 74 | ... |
| 2011 Sep 8.1 | 3.1 | 497 ± 65 | A |
| ... | 5.0 | 279 ± 50 | ... |
| ... | 8.5 | 182 ± 47 | ... |
| 2011 Oct 11.0 | 5.0 | 411 ± 22 | D |
| ... | 6.8 | 332 ± 19 | ... |
| ... | 8.4 | 290 ± 26 | ... |
| 2011 Dec 3.9 | 5.0 | 256 ± 30 | D |
| ... | 6.8 | 168 ± 19 | ... |
| ... | 8.4 | 219 ± 19 | ... |
| 2012 Jan 29.8 | 5.0 | 272 ± 26 | C |
| ... | 6.8 | 197 ± 18 | ... |
| ... | 8.4 | 124 ± 20 | ... |
| 2012 Mar 10.6 | 2.5 | 268 ± 41 | C |
| ... | 3.5 | 330 ± 30 | ... |
| ... | 5.0 | 199 ± 20 | ... |
| ... | 6.8 | 116 ± 15 | ... |
| ... | 8.4 | 130 ± 16 | ... |

We also obtained radio observations of SN 2011ei beginning shortly after explosion. On 2011 August 3.2, we observed SN 2011ei with the Karl G. Jansky Very Large Array (VLA; Perley et al. 2011) at frequencies of $\nu = 5$ and 25 GHz. Following a strong detection of radio emission at 5 GHz (Chomiuk & Soderberg 2011), we initiated an VLA monitoring campaign at frequencies spanning 2-9 GHz to obtain observations between August 2011 - March 2012 (PI Soderberg; 10C-168, 11B-212).

All VLA observations were obtained with the widest bandwidth available at any time during the commissioning phase. Prior to 2011 October 1 this amounted to two 128-MHz wide sub-bands (total bandwidth of 256 MHz), while we later utilized the total bandwidth of 2 GHz at S- and C-bands; in the latter case the central frequencies were tuned to 5.0 and 6.8 GHz. Given that fully upgraded X-band receivers were not yet available, our observations at this band spanned 8.0-8.8 GHz. We used J2101-2933 as a phase-calibrator source and 3C48 for flux calibration. Initial observations were obtained in the extended A-configuration while later observations were obtained in the compact C- and D-configurations.

Data were reduced using the standard packages of the Astronomical Image Processing System (AIPS). In each observation, we fit a Gaussian to the source and extracted the integrated flux density. For observations in the compact D-array we limited the uv-range ($\gtrsim 5$ k λ) to minimize contamination from diffuse host galaxy emission. Our final flux density measurements for SN 2011ei are reported in Table 4.

3. PROPERTIES OF THE UV, OPTICAL, AND BOLOMETRIC LIGHT CURVES

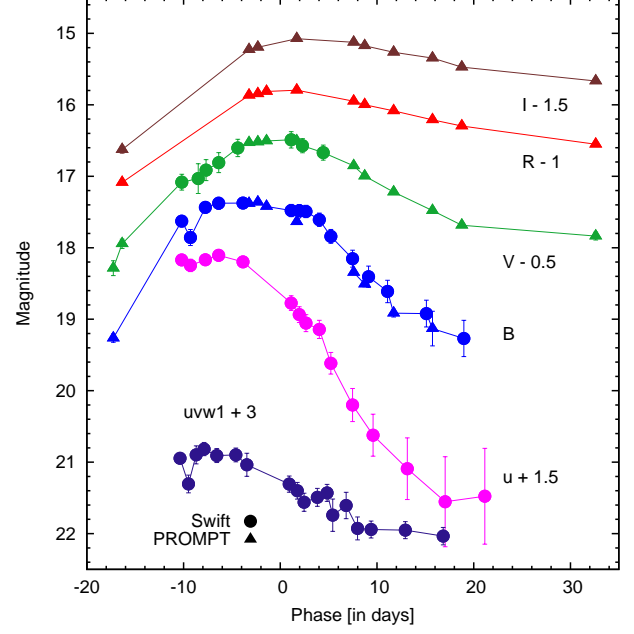


Figure 3. Observed *Swift*-UVOT and PROMPT light curves of SN 2011ei. Light curves have been shifted by indicated amounts for clarity.

Table 5
Epoch of maximum light and peak magnitude for the light curves of SN 2011ei

| Filter | Peak Time (UT) | Peak Time (JD-2400000) | Peak Obs. (m(λ)) _{max} |
|-------------|----------------|------------------------|-------------------------------------------|
| <i>uvw1</i> | 2011 Aug 05.0 | 55778.5 ± 2.0 | 17.8 ± 0.10 |
| <i>u</i> | 2011 Aug 06.0 | 55779.5 ± 1.5 | 16.6 ± 0.10 |
| <i>B</i> | 2011 Aug 10.0 | 55783.5 ± 2.0 | 17.4 ± 0.05 |
| <i>V</i> | 2011 Aug 13.0 | 55786.5 ± 1.5 | 17.0 ± 0.05 |
| <i>R</i> | 2011 Aug 13.5 | 55787.0 ± 1.5 | 16.8 ± 0.07 |
| <i>I</i> | 2011 Aug 16.0 | 55789.5 ± 1.5 | 16.6 ± 0.07 |

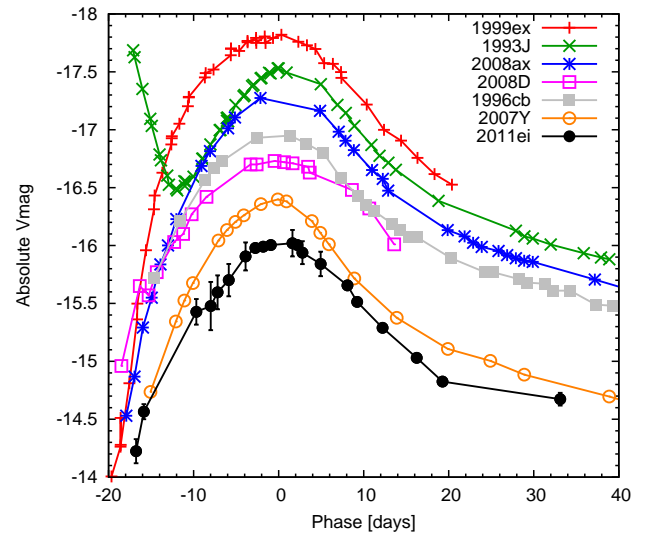


Figure 4. V-band absolute light curve of SN 2011ei compared to light curves of Type IIb and Ib objects: SN 1999ex (Type Ib; Stritzinger et al. 2002), SN 1993J (Type IIb; Lewis et al. 1994), SN 2008ax (Type IIb; Pastorello et al. 2008), SN 1996cb (Type IIb; Qiu et al. 1999), and SN 2007Y (Type Ib; Stritzinger et al. 2009).

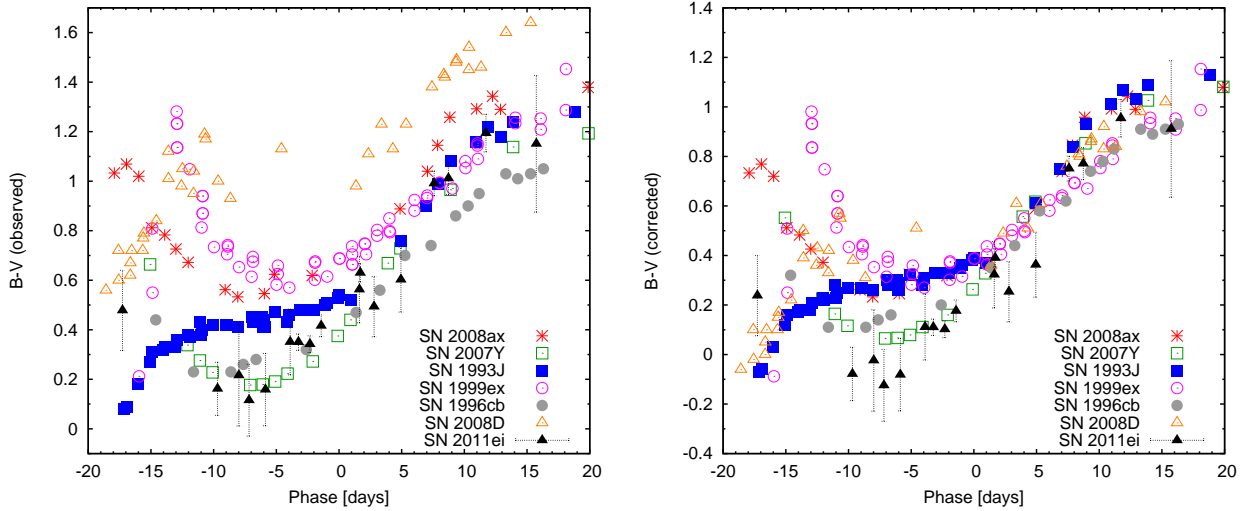


Figure 5. The $B - V$ color curves of SN 2011ei compared to those of other stripped-envelope SNe: SN 2008ax (Type IIb; Pastorello et al. 2008), SN 2007Y (Type Ib; Stritzinger et al. 2009), SN 1993J (Type IIb; Lewis et al. 1994), SN 1999ex (Type Ib; Stritzinger et al. 2002), SN 1996cb (Type IIb; Qiu et al. 1999), and SN 2008D (Type Ib; Mazzali et al. 2008). On the left are observed colors, and on the right are colors corrected for extinction.

3.1. UV and Optical Light Curves and Colors

Figure 3 shows the observed *Swift*-UVOT and PROMPT light curves of SN 2011ei. The properties of these curves are presented in Table 5. The time and observed magnitude at maximum light of each filter light curve were estimated with low-order polynomials. The average time to rise to peak brightness from the time of explosion (t_{exp}) for SNe IIb and Ib in the V -band is $\Delta t_{\text{exp}} \lesssim 20$ d (Richardson et al. 2006; Drout et al. 2011). Thus, our discovery observation is likely to have been obtained within ~ 1 day of outburst and we adopt an explosion date of July 25.0 hereafter.

In Figure 4, the absolute V -band light curve of SN 2011ei is compared with those of well observed SNe IIb and Ib. With a peak absolute magnitude of $M_V \approx -16$ mag, SN 2011ei was approximately 2 mag below the mean peak absolute magnitudes of the entire class of stripped-envelope events (Richardson et al. 2006; Drout et al. 2011). Other low-luminosity events include the Type Ib SN 2007Y ($M_V = -16.5$; Stritzinger et al. 2009), and SN 2008D ($M_V = -16.7$; Soderberg et al. 2008).

A significant difference between SN 2011ei and SN 1993J clearly illustrated in Figure 4 is that SN 2011ei does not show the prominent early-time peak exhibited by the light curve of SN 1993J. This peak is presumably attributed to the initial shock heating and subsequent cooling of a low-mass envelope of a star with radius $\sim 4 \times 10^{13}$ cm (Bartunov et al. 1994; Shigeyama et al. 1994; Woosley et al. 1994). The lack of a noticeable early-time rise suggests SN 2011ei had a smaller envelope than SN 1993J. The implications for the progenitor radius are further investigated in Section 3.4.

In Figure 5, the observed $(B - V)$ color curve of SN 2011ei with respect to V -band maximum is plotted along with those of other SNe IIb and Ib. Also shown are the same color curves corrected for extinction. Like SN 1999ex and SN 2008ax, the $(B - V)$ colors of SN 2011ei first become increasingly blue in the days immediately following outburst. Then, around 5–10 days before maximum, the SN becomes redder with time and the colors

increase monotonically. The majority of $(B - V)$ color indices of SN 2011ei are somewhat bluer than those of other SNe after correction. This blue excess suggests that the adopted $E(B - V) = 0.24$ mag is likely an upper limit.

3.2. Bolometric Light Curve

The extinction-corrected *Swift*-UVOT and PROMPT light curves were combined to obtain a quasi-bolometric light curve ($L_{\text{bol}}^{\text{quasi}}$) of SN 2011ei. Low-order polynomials have been used to interpolate the light curves. The total UV+ BVR I flux was determined by summing the integrated fluxes of the different filters and uncertainties have been propagated following standard practice.

The quasi-bolometric UV+ BVR I light curve was then transformed into a bolometric light curve assuming $L_{\text{bol}}^{\text{quasi}} \approx 0.8L_{\text{bol}}$. The remaining $0.2L_{\text{bol}}$ goes into unobserved near infrared emission. This estimate is in line with bolometric reconstructions of SNe IIb and Ib with extensive observations such as SN 2007Y (Stritzinger et al. 2009), SN 2008ax (Pastorello et al. 2008; Taubenberger et al. 2011), and SN 2008D (Mazzali et al. 2008; Soderberg et al. 2008).

The final bolometric light curve of SN 2011ei is shown in Figure 6. Also shown in the figure are the bolometric light curves of SN 1999ex, 1993J, 2007Y, and 2008D. The bolometric light curve peaks ≈ 14.4 days after outburst with $L_{\text{bol}} \sim 7 \times 10^{41}$ ergs $^{-1}$, making SN 2011ei one of the least luminous SNe IIb/Ib observed to date. Among the closest in luminosity is SN 2007Y which peaked at $L_{\text{bol}} \sim 1.3 \times 10^{42}$ ergs $^{-1}$.

3.3. Explosion Parameters

Modeling of the bolometric light curve was used to infer the ejecta mass (M_{ej}), the nickel mass (M_{Ni}) and the kinetic energy of the ejecta (E_k). Following the procedures of Valenti et al. (2008), we assumed the early-time ($\Delta t_{\text{exp}} < 40$ d) light curve to correspond with the photospheric regime and adopted a constant optical opacity $k_{\text{opt}} = 0.07 \text{ cm}^2 \text{ g}^{-1}$ which is valid so long as electron scattering is the dominant opacity source and the ejecta are triply ionized (see, e.g., Chugai 2000). At late times

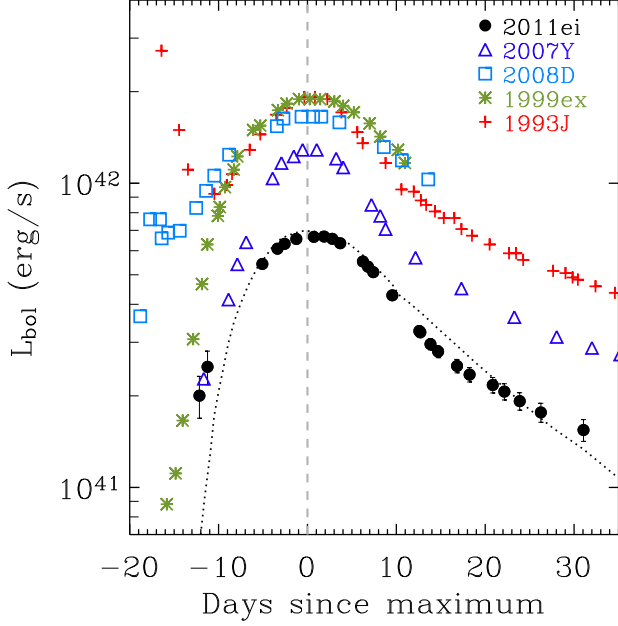


Figure 6. Reconstructed bolometric light curve of SN 2011ei compared to those of SN 2007Y (Type Ib; Stritzinger et al. 2009), SN 2008D (Type Ib; Mazzali et al. 2008), SN 1999ex (Type Ic; Stritzinger et al. 2002), and SN 1993J (Type IIb; Richmond et al. 1994). Plotted over the points for SN 2011ei is the final best-fit curve used to determine explosion parameters. Phase is with respect to the peak of SN 2011ei’s bolometric light curve, which occurs on 2011 August 08.4 (JD 2456147.9).

($\Delta t_{\text{exp}} > 40$ d) the optical depth of the ejecta decreases and the observed luminosity is powered by γ -rays arising from the ^{56}Co decay, γ -rays from electron-positron annihilation, and the kinetic energy of the positrons (Sutherland & Wheeler 1984; Cappellaro et al. 1997).

From the above modeling scheme the following best-fitting parameters were derived: $M_{\text{ej}} \sim 1.6 M_{\odot}$, $E_k \sim 2.5 \times 10^{51}$ erg, and $M_{\text{Ni}} = 0.030 \pm 0.005 M_{\odot}$. Our model under-predicts the observed luminosity at early times ($\Delta t_{\text{exp}} < 5$ d). This suggests the presence of an additional component of emission. We explore the possibility of cooling envelope emission following shock break-out in Section 3.4.

As an independent check we note that our best-fitting explosion parameters imply a photospheric velocity, v_{ph} , at peak luminosity of

$$v_{\text{ph}} \approx \left(\frac{6E_k}{5M_{\text{ej}}} \right)^{0.5} \sim 10,000 \text{ km s}^{-1},$$

which is in agreement with the expansion velocities observed in the optical spectra (see Section 4.1). A separate check of the Ni mass comes from a relationship between M_{Ni} vs. peak absolute R -band magnitude (M_R) presented in Drout et al. (2011). SN 2011ei’s extinction-corrected peak of $M_R \approx -16.1$ mag yields a model-derived Ni mass of $M_{\text{Ni}} < 0.04 M_{\odot}$, which is consistent with our result.

3.4. Radius of the Progenitor Star

The fortuitous discovery of SN 2011ei not long after outburst enabled us to trace the temporal evolution of the early optical emission (see Figure 3). As discussed by Ensmann & Burrows (1992), the optical emission from

core-collapse SNe in the first few days after explosion is dominated by adiabatic cooling of the outer envelope material following the break-out of the forward shock. This component can be roughly approximated by a blackbody spectrum with a radius and temperature determined by the ejecta parameters, M_{ej} and E_k (see Chevalier & Fransson 2008 and Nakar & Sari 2010 for a detailed discussion). In turn, these parameters enable an estimate of the progenitor radius, R_* .

The first R -band detection of SN 2011ei was made shortly after explosion with luminosity, $L_R \approx 2.4 \times 10^{40} \text{ erg s}^{-1}$. This initial observation was used to constrain the radius of the progenitor star by modeling the cooling envelope emission, adopting the formalism of Chevalier & Fransson (2008). In this scenario, the temperature of the photosphere is

$$T_{\text{ph}} \approx 7800 E_{k,51}^{0.03} M_{\text{ej},\odot}^{-0.04} R_{*,11}^{0.25} \Delta t_{\text{exp}}^{-0.48} \text{ K}, \quad (1)$$

and the photospheric radius is

$$R_{\text{ph}} \approx 3 \times 10^{14} E_{k,51}^{0.39} M_{\text{ej},\odot}^{-0.28} \Delta t_{\text{exp}}^{0.78} \text{ cm}. \quad (2)$$

Here we have normalized $E_{k,51}$ to 10^{51} erg, $M_{\text{ej},\odot}$ to M_{\odot} , $R_{*,11}$ to 10^{11} cm, and Δt_{exp} is in days since explosion.

For explosion parameters determined in Section 3.3 and the adopted explosion date 2011 July 25.0, the extinction-corrected discovery magnitude constrains $R_* \lesssim 10^{11}$ cm. This estimate is consistent with upper limits on the progenitor radius derived from a similar analysis of the first B - and V -band detections ~ 2.5 days after explosion (see Table 1). Thus, the early optical emission points to a compact progenitor, similar to those of SNe Ibc and compact IIb (Chevalier & Soderberg 2010).

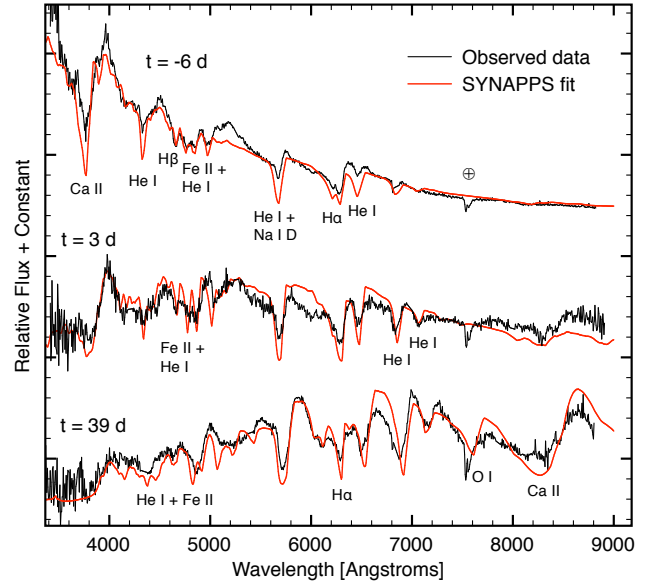


Figure 7. Representative SYNAPPS fits to optical spectra of SN 2011ei. Phase is with respect to V -band maximum.

4. OPTICAL SPECTROSCOPY

Properties of the optical spectra of SN 2011ei are described and compared with other stripped-envelope

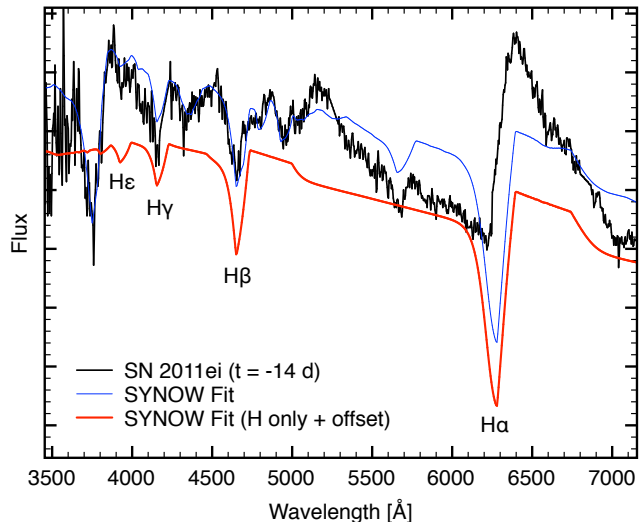


Figure 8. Attempted SYNOW fits of $t = -14$ d spectrum of SN 2011ei. The blue line represents the complete model and the red line represents the model only using hydrogen. Features blueward of 5000 Å are fit reasonably well, but none of the models we tried fit the broad H α profile.

events below. The dates of spectroscopic observations are referenced as $t = x$, where x is the phase with respect to V-band maximum; negative numbers are pre-maximum, and positive numbers are post-maximum.

Line identifications and estimates of expansion velocities were made with the supernova spectrum synthesis code SYNOW. Manual and automated procedures employing the recently updated versions of the software SYN++ in combination with SYNAPPS were used.⁴ The basic assumptions of SYNOW include spherical symmetry, velocity proportional to radius, a sharp photosphere, line formation by resonant scattering treated in the Sobolev approximation, local thermodynamic equilibrium (LTE) for the level populations, no continuum absorption, pure resonance scattering, and only thermal excitations. Fits are constrained by how we are able to best match absorption minimum profiles, as well as the relative strengths of all the features (see Branch et al. 2002 for more description of fitting parameters and Thomas et al. 2011 for software details). Representative SYNAPPS fits are shown in Figure 7.

4.1. Early Spectral Evolution

SN 2011ei evolved rapidly in its pre-maximum light optical spectra. The earliest spectrum ($t = -14$ d; Figure 8) shows strong Type II-like hydrogen P-Cygni features. The H α profile exhibits a ‘saw-toothed’ shape, rising steeply from a minimum at 6220 Å ($-16,000$ km s $^{-1}$) to a maximum at 6395 Å. Redshifted emission extends to approximately 7000 Å ($+19,000$ km s $^{-1}$). In Figure 8, two SYNOW synthetic fits to the $t = -14$ d spectrum of SN 2011ei are shown: one a complete model, and the other using only hydrogen. The H β , H γ , and H ϵ absorptions are fit reasonably well with a velocity of 14,500 km s $^{-1}$. Additional features in this spectrum are fit with Ca II, Na I, and Fe II. Attempts to produce satisfactory fits of the H α profile failed, likely due to the LTE and resonance scattering assumptions of SYNOW.

⁴ Software was retrieved from <https://c3.lbl.gov/es/>

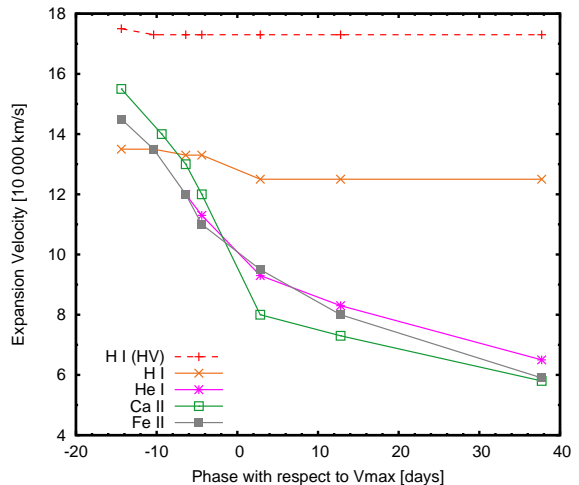


Figure 9. Expansion velocities of prominent ions in the spectra of SN 2011ei determined from SYNOW fitting. Uncertainties in velocity estimates are ~ 500 km s $^{-1}$. The identification of high-velocity (HV) H I is poorly constrained since it is observed only in H α .

In the next two spectra on $t = -10$ and $t = -6$ d, the prominent H α emission profile subsides and the spectra instead exhibit conspicuous He absorptions usually associated with SNe Ib. The continuum becomes increasingly blue and the He I $\lambda 5876$, $\lambda 6678$, $\lambda 5016$, and $\lambda 7065$ lines appear but are weak and narrow. Blueshifted absorption of the H α line around 6250 Å develops two minima. The center of the trough sits around the observed wavelength of 6300 Å so contamination from the [O I] $\lambda 6300$ night sky line is possible. However, the peak between the two absorptions is fairly strong and shows a distribution as opposed to a narrow, unresolved line associated with telluric emission.

The 6250 Å feature was modeled using two components of hydrogen at velocities of $\approx 17,000$ km s $^{-1}$ and 14,000 km s $^{-1}$. Though two distinct absorptions are observed around H α , only one conspicuous absorption is observed around H β . The SYNOW fit confirms that two components of hydrogen with a velocity difference of ~ 3000 km s $^{-1}$ blend together and manifest as a single feature in all Blamer lines except H α . Attempts to fit with other ions such as Si II, Ne I, and C II introduced inappropriate features elsewhere in the synthetic spectra and/or were at velocities well below the photosphere and were considered unsuccessful. The properties of this absorption as observed in SN 2011ei and a number of stripped-envelope events is explored further in Section 4.4.

From $t = -6$ to $t = +3$ d, the He I lines strengthen. High-velocity calcium absorption is not detected in the early spectra, which is interesting given that it has been reported at these epochs in several SNe Iib and Ib including SN 1999ex, SN 2005bf, SN 2007Y, and SN 2008ax (Stritzinger et al. 2002; Folatelli et al. 2006; Stritzinger et al. 2009), but not in SN 2008D (Modjaz et al. 2009). Emission around 8700 Å associated with the infrared Ca II triplet is noticeable shortly after maximum light and then gradually strengthens in the following months.

Additional ions outside of H I, He I, Ca II, Na I, and Fe II were introduced to the synthetic spectra to model the $t = 39$ d spectrum. The most conspicuous change

is O I absorption around 7600 Å. Additional absorptions are fit using a blend of S II features around 5200 Å, Si II λ 6355, and Ba II λ 6142 and λ 6496, however, their removal do not change any conclusions reported here and are not considered significant.

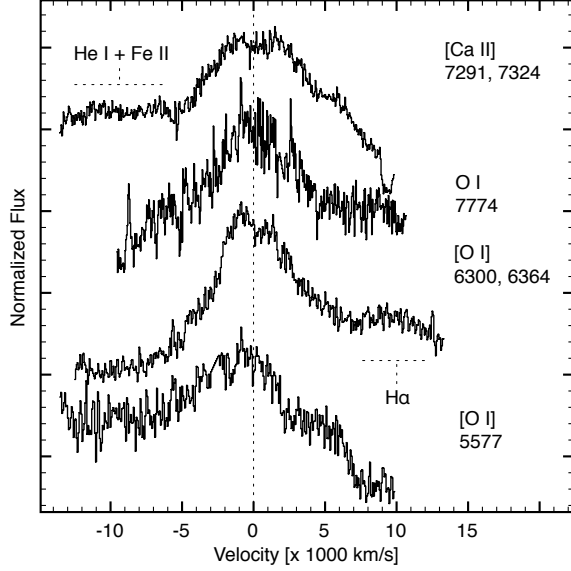


Figure 10. Late-time emission line profiles of SN 2011ei from the $t = 97$ d spectrum. Instances where line profiles are contaminated by emissions from other lines are indicated.

The evolution in the expansion velocities for the most prominent ions in SN 2011ei as estimated from the SYNOW fitting is shown in Figure 9. Some noteworthy trends are observed. The high-velocity hydrogen shows almost no change over all of the sampled epochs, and the second, lower-velocity hydrogen component shows a slight drop before leveling out after maximum light. The remaining ions He I, Ca II, and Fe II show velocities that drop most steeply before maximum light, after which the rate of velocity change decreases. The expansion velocities of the He I and Fe II ions closely follow each other.

4.2. Nebular Phase Spectrum

Starting with the $t = 74$ d spectrum, emission from forbidden transitions is apparent and SN 2011ei begins to enter the nebular phase. The broad ≈ 6250 Å absorption is no longer observed and in its place is an emission feature associated with [O I] $\lambda\lambda$ 6300, 6364. Prominent emission from [O I] λ 5577, [Ca II] $\lambda\lambda$ 7291, 7324, and O I λ 7774 is also observed, typical of other SNe at these epochs. Mg I λ 4571 is not observed, possibly because of line blending with Fe II and/or low ionic fraction.

In Figure 10, emission line profiles of the $t = 97$ d late-time spectrum of SN 2011ei are enlarged and plotted in velocity space. All oxygen emissions show a slight bulk blueshift (≈ -600 km s $^{-1}$). The fairly broad [Ca II] $\lambda\lambda$ 7291, 7324 emission has a flat top centered around zero velocity (assumed to lie around 7306 Å), with a blueward ledge that is probably a combination of He I λ 7065 and [Fe II] λ 7155. Redshifted [O I] $\lambda\lambda$ 6300, 6364 emission blends with H α emission attributable to high-velocity hydrogen gas interacting with dense circumstellar material

(Houck & Fransson 1996).

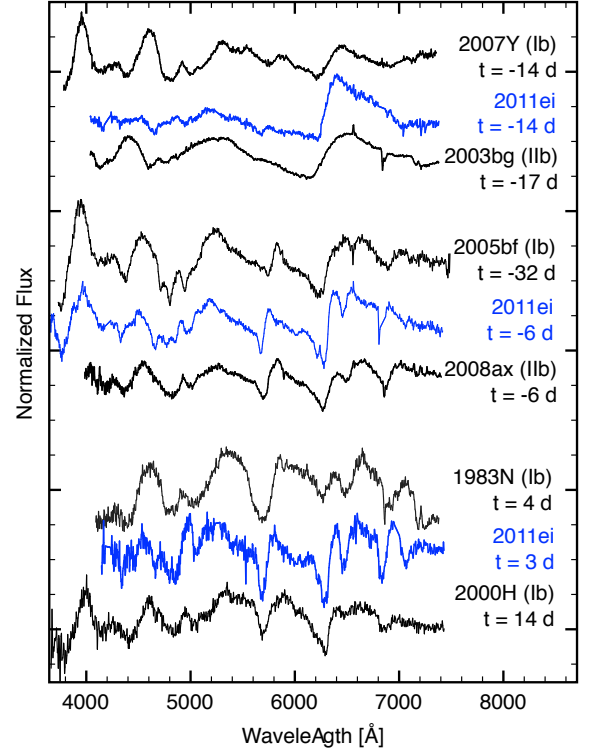


Figure 11. Early spectra of SN 2011ei compared to those of other SNe I Ib and Ib. Spectra have been normalized according to the procedure outlined in Jeffery et al. (2007) to aid in visual comparison.

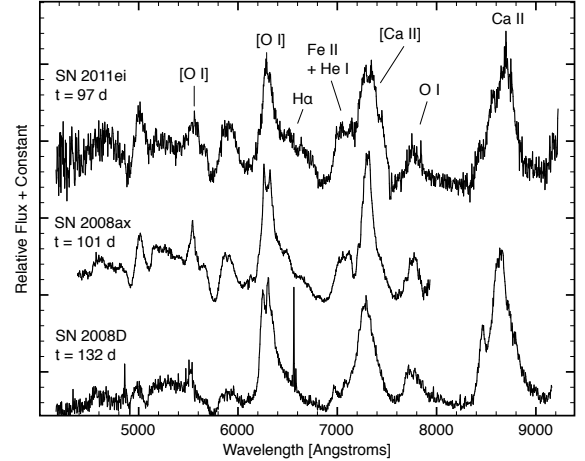


Figure 12. Late-time optical spectra of SN 2011ei compared to spectra of SN 2008ax (Milisavljevic et al. 2010) and SN 2008D (Modjaz et al. 2009). O I λ 8446 may contribute to strong emission observed around the Ca II infrared triplet.

4.3. Comparison to SNe I Ib and Ib

SN 2011ei shares spectral properties with many SNe I Ib and Ib. Selected examples are plotted in Figure 11. The earliest spectrum ($t = -14$ d) shows close similarity to that of SN 2007Y (Stritzinger et al. 2009). Both SNe exhibit a rarely-observed, extended, high-velocity H α profile that dominates the spectrum. However,

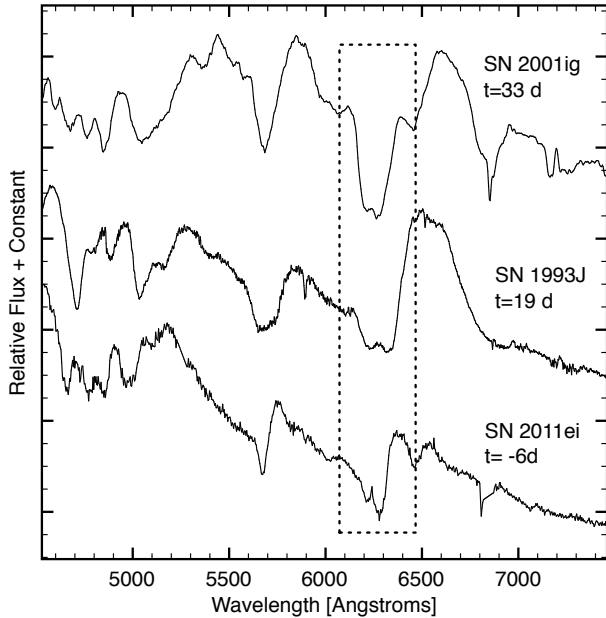


Figure 13. Evidence of two-component absorption centered near ≈ 6250 Å for SN 2001ig, SN 1993J (Matheson et al. 2000), and SN 2001ig (Silverman et al. 2009). Phase is with respect to V -band maximum. The dashed box highlights the region around $H\alpha$ where the absorption is observed.

SN 2011ei does not have the broad calcium absorption seen in SN 2007Y around 8400 Å, nor does it show the pronounced features between 4000 – 5000 Å associated with Fe II and He I. A likeness between SN 2011ei and SN 2003bg is also seen (Hamuy et al. 2009; Mazzali et al. 2009). In this case, the $H\alpha$ profiles are comparable, but SN 2003bg shows a blueshifted absorption associated with higher velocities ($\sim 20,000$ km s $^{-1}$) and distributed more gradually. As with SN 2007Y, the features blueward of 5000 Å are more pronounced in SN 2003bg than in SN 2011ei.

Approximately one week before maximum light, when the $H\alpha$ emission is no longer conspicuous in SN 2011ei, its spectra resemble those of SNe IIB from compact progenitors and SNe Ib exhibiting absorption around ≈ 6250 Å. Shown in Figure 11 (*middle section*) is the Type Ib SN 2005bf (Folatelli et al. 2006) early in its unusual late-peaking light curve, and the Type IIB SN 2008ax (Pastorello et al. 2008) at $t = -6$ d. By the time of maximum light and in the months that follow, SN 2011ei continues to exhibit spectral properties consistent with those of SNe Ib. Other examples plotted in Figure 11 (*bottom section*) are SN 1983N (Harkness et al. 1987) and SN 2000H (retrieved electronically via SUSPECT courtesy of the Asiago SN Group). Among all the SNe IIB and Ib examined, SN 2011ei has among the narrowest line features, particularly in its hydrogen and helium lines.

The overall emission properties of SN 2011ei at nebular epochs are also quite similar to those of SNe IIB and Ib. This is clear in Figure 12, where the $t = 97$ d spectrum of SN 2011ei is compared to spectra of SN 2008D and SN 2008ax at similar epochs. However, one noticeable difference is that [Ca II] $\lambda\lambda 7291, 7324$ emission in SN 2011ei is broader and more box-like compared to those of other SNe. Box-like profiles are associated with

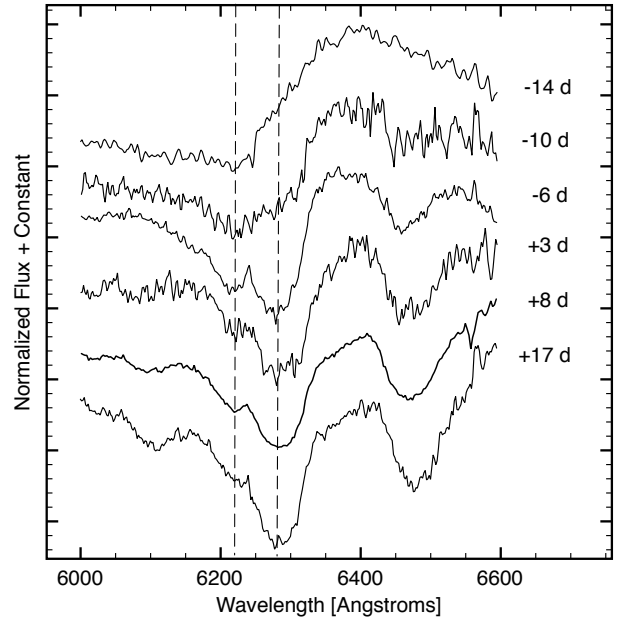


Figure 14. Time series spectra of SN 2011ei in the region of $H\alpha$ showing evidence for two-component absorption evolution. The dashed lines mark the individual components.

emission from material arranged in a thick shell.

In contrast with some stripped-envelope events like SN 2008D and SN 2008ax that show conspicuous, multiple peaks in their [O I] $\lambda\lambda 6300, 6364$ emission (see, e.g., Mazzali et al. 2005; Modjaz et al. 2008, 2009; Maeda et al. 2008; Taubenberger et al. 2009; Milisavljevic et al. 2010), no narrow and/or conspicuous line substructure is observed in SN 2011ei. However, SN 2011ei is not fully nebular in the presented spectrum, and some SNe IIB and Ibc do not show strong asymmetric peaks until $t > 200$ d (e.g., SN 2009jf; Valenti et al. 2011). A small absorption in the [O I] $\lambda\lambda 6300, 6364$ profile around 6305 Å is suggestive of clumpy ejecta. However, the profile may be influenced by the high-velocity $H\alpha$ absorption observed at early epochs (Maurer et al. 2010).

The spectroscopic similarity of SN 2011ei to other SNe IIB and Ib permits an estimate to be made of the mass of hydrogen contained in the thin H-rich envelope surrounding the progenitor star prior to outburst. James & Baron (2010) investigated the Type Ib SN 1999dn and SN 2000H using the non-LTE (NLTE) stellar atmospheres code PHOENIX. They derived estimates of $M_H \lesssim 10^{-3} M_\odot$ and $M_H \lesssim 0.2 M_\odot$ for these SNe, respectively, assuming solar metallicity. The strength and duration of $H\alpha$ line absorption observed in SN 2011ei falls in between these events, suggesting an H mass in the region of $\sim 0.01 M_\odot$. This estimate is consistent with recent radiative transfer models carried out in NLTE conditions by Hachinger et al. (2012) who find that the H mass that distinguishes between SN IIB and Ib to be $0.025 - 0.033 M_\odot$. Our estimate also places SN 2011ei in the same range of H mass estimates for SN 2008ax (Chornock et al. 2011), which shares many spectroscopic similarities.

4.4. Multi-component Absorption Due to Hydrogen

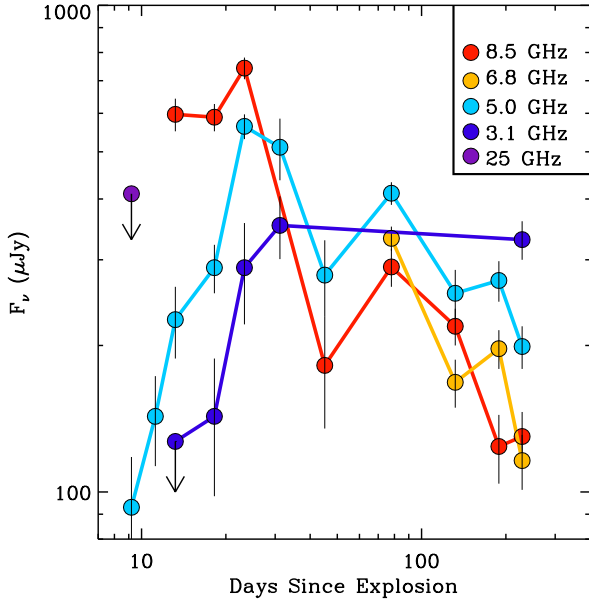


Figure 15. VLA radio light curves of SN 2011ei are shown at frequencies spanning 3.1 to 25 GHz. At the best sampled frequency, 5 GHz, we find evidence for a secondary maximum at $\Delta t_{\text{exp}} \approx 80$ days that is also seen in the 8.4 GHz light curve.

The two-minima absorption observed around 6200 – 6300 Å is not unique to SN 2011ei. In Figure 13, we show spectra of SN 2011ei, SN 1993J and SN 2001ig that illustrate how these events all share broad absorption suggestive of two components. The epochs at which this phenomenon is visible ranges considerably from $t = 33$ d in SN 2001ig, to $t = 19$ d in SN 1993J, to $t = -6$ d in SN 2011ei. In the case of SN 2011ei, there is clear evolution in the relative strength of the two components. The blueward absorption is observed first, then the second, redward absorption appears and increases in strength (see Figure 14).

The interpretation of the two-component feature is not clear. Its nature in SN 1993J has been investigated thoroughly using SYNOW spectral fitting and NLTE modeling (Baron et al. 1994, 1995; Zhang et al. 1995b,a; Zhang & Wang 1996). Suspected origins include ejecta asymmetry, mixture with Fe II or Si II lines, and a complicated two-component density structure in H-rich material. James & Baron (2010) found that they were unable to model a similar two-component feature in the Type Ib SN 2000H and attributed it to be due in part to interaction with circumstellar material (CSM). They cited a quickly-fading Na I D feature between two spectra obtained around maximum light as evidence for environmental interaction. More recently, Hachinger et al. (2012) attributed the feature in SNe IIb and Ib to a blend of high-velocity H α and Si II.

Multi-component absorption may be a common phenomenon across supernova types and emission lines. For example, evidence for two components of high-velocity hydrogen absorption has been seen in early spectra of the Type Ib SN 1999dn (Benetti et al. 2011), as well as the Type IIb SN 2011dh during the first month following outburst (H. Marion, private communication, 2012). Multi-component absorption has also been recognized in the com-

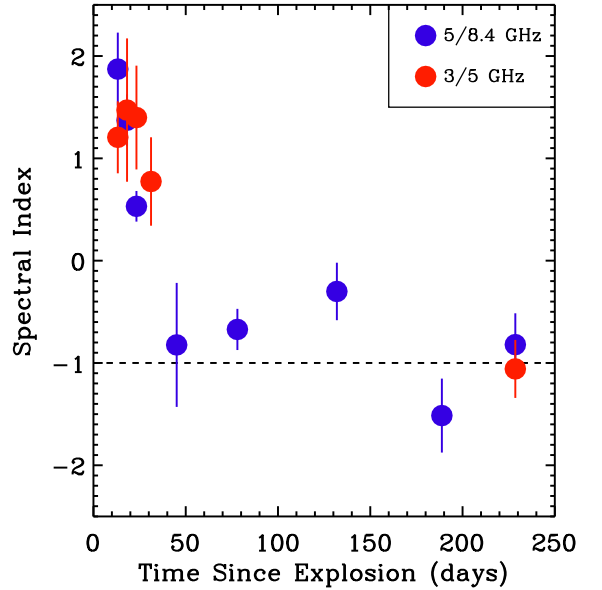


Figure 16. The evolution of the radio spectral indices spanning 3 to 8.4 GHz are shown. The early radio emission is optically thick, $F_\nu \propto \nu^2$, but gradually evolves to an optically thin spectrum, $F_\nu \propto \nu^{-1}$.

plex evolution of broad Si II $\lambda 6355$ and Ca II H&K absorption features in Type Ia supernovae (Foley et al. 2011, 2012).

4.5. Explosion Site Metallicity

Possible metallicity differences between SN subtypes and their relation to progenitor systems is currently an active area of investigation (e.g., Prieto et al. 2008; Arcavi et al. 2010; Anderson et al. 2010; Modjaz et al. 2011; Kelly & Kirshner 2011; Sanders et al. 2012). This motivated estimates of the metallicity of the host environment region of SN 2011ei to be made. Because no strong narrow nebular lines were observed in the spectra aside from a relatively weak detection of H α , an emission line region located $\approx 3''4$ (≈ 470 pc) north from SN 2011ei in our 2011 November 17 observation was extracted. From this spectrum, nebular emission lines of H α , H β , [N II] $\lambda\lambda 6548, 6583$ and [O III] $\lambda\lambda 4959, 5007$ were clearly detected and their relative strengths measured after correcting for extinction.

From the O3N2 diagnostic of Pettini & Pagel (2004), we estimate an oxygen abundance of $\log(\text{O}/\text{H}) + 12 = 8.44$. A slightly higher value of $\log(\text{O}/\text{H}) + 12 = 8.57$ is determined using their N2 diagnostic. The statistical uncertainty in these metallicity estimates is much smaller than the systematic error associated with the diagnostics; e.g. ~ 0.07 dex for the O3N2 diagnostic, as determined by Kewley & Ellison (2008) via comparison to other strong line abundance indicators.

Adopting a solar metallicity of $\log(\text{O}/\text{H})_\odot + 12 = 8.69$ (Asplund et al. 2005), our measurement suggests that the environment of SN 2011ei has a sub-solar metallicity of around $Z \approx 0.6 Z_\odot$. We note that this result is not unlike sub-solar metallicities estimated for other SNe IIb (see, e.g., Kelly & Kirshner 2011; Modjaz et al. 2011; Sanders et al. 2012).

5. RADIO AND X-RAY DIAGNOSTICS

5.1. Radio Light Curves, Forward Shock, and Magnetic Field

While optical data probe the thermal emission from the slow moving bulk ejecta, non-thermal synchrotron emission in the radio is produced as the forward shock races ahead and dynamically interacts with the CSM. Radio observations can thus provide unique information about the progenitor star's mass-loss history several years to centuries immediately prior to outburst.

We show the observed radio light curves of SN 2011ei in Figure 15. The radio light curves show flux density variations of a factor of ~ 3 with a 5 GHz peak luminosity, $L_\nu \approx 6.2 \times 10^{26} \text{ erg s}^{-1} \text{ Hz}^{-1}$, approximately 23 days after explosion. Compared to other SNe I Ib and Ibc (e.g., SN 2011dh; Soderberg et al. 2011; Krauss et al. 2012), the peak radio emission from SN 2011ei is fairly weak. Approximately 40 days after outburst, the radio emission decays steeply at all frequencies, then rises again to a second maximum ~ 3 months post-explosion.

As the forward shock expands into the surrounding environment, electrons are accelerated to relativistic velocities with a distribution, $N(\gamma_e) \propto \gamma_e^{-p}$, where γ_e is the Lorentz factor of the particles. Amplified magnetic fields cause the shocked electrons to gyrate and emit synchrotron emission detectable in the cm-band on a timescale of days after the explosion (Chevalier 1982). A low frequency spectral turnover has been observed for radio SNe Ibc and I Ib attributed to synchrotron self-absorption defining a spectral peak, ν_a , and characterizes the spectrum as $F_\nu \propto \nu^{5/2}$ below ν_a and $F_\nu \propto \nu^{-(p-1)/2}$ above ν_a . At the epoch ν_a crosses each observing band(s), the radio light curve reaches maximum intensity.

In Figure 16, we show the radio spectral indices in adjacent bands spanning 3 to 8 GHz for SN 2011ei. The early radio emission is absorbed with $F_\nu \propto \nu^2$ while the later emission is optically thin with approximately $F_\nu \approx \nu^{-1}$, implying $p \approx 3$. As shown in Figure 15, the 5 GHz light curve peaks on 2011 August 17 ($\Delta t_{\text{exp}} \approx 23$ days) with a flux density of $F_{\nu,p} \approx 560 \mu\text{Jy}$. Adopting $p = 3$, we estimate the time-averaged velocity, $\bar{v} \equiv R/\Delta t$, of the forward shock to be,

$$\begin{aligned} \bar{v} \approx 0.14c \times (\epsilon_e/\epsilon_B)^{-1/19} (F_{\nu,p}/\text{mJy})^{9/19} \\ \times (d/10 \text{ Mpc})^{18/19} (\nu_p/5 \text{ GHz})^{-1} \\ \times (t_p/10 \text{ days})^{-1}, \end{aligned} \quad (3)$$

or $\bar{v} \approx 0.13c$ (see Chevalier & Fransson 2006).

Here we have assumed that half of the volume enclosed by the forward shock is producing synchrotron emission⁵, and ϵ_e and ϵ_B represent the efficiency of the shock wave in accelerating electrons and amplifying magnetic fields, respectively. We have further assumed that the shock is in equipartition (defined as $\epsilon_e = \epsilon_B$). The inferred shock wave velocity for SN 2011ei is in line with the ve-

⁵ Very long baseline interferometry radio images of SN 1993J suggested a spherical shell structure with a shell thickness 20-33% of the outer radius (Bietenholz et al. 2011; Martí-Vidal et al. 2011), in which case 49-70% of the volume enclosed by the forward shock is filled with radio emission. However, possible small scale clumpiness within this geometry could lower the effective radio-emitting volume.

locities derived for SNe Ibc and compact progenitor SNe I Ib (Chevalier & Soderberg 2010; Soderberg et al. 2011), and higher than those inferred for extended progenitor SNe I Ib and SNe of Type IIP (Chevalier 1998).

Following Chevalier & Fransson (2006), we find the strength of the amplified magnetic field (B) for the radio emitting material to be

$$\begin{aligned} B \approx 0.68 \times G (\epsilon_e/\epsilon_B)^{-4/19} (F_{\nu,p}/\text{mJy})^{-2/19} \\ \times (d/10 \text{ Mpc})^{-4/19} (\nu_p/5 \text{ GHz}), \end{aligned} \quad (4)$$

or $B \approx 0.6 \text{ G}$ for equipartition.

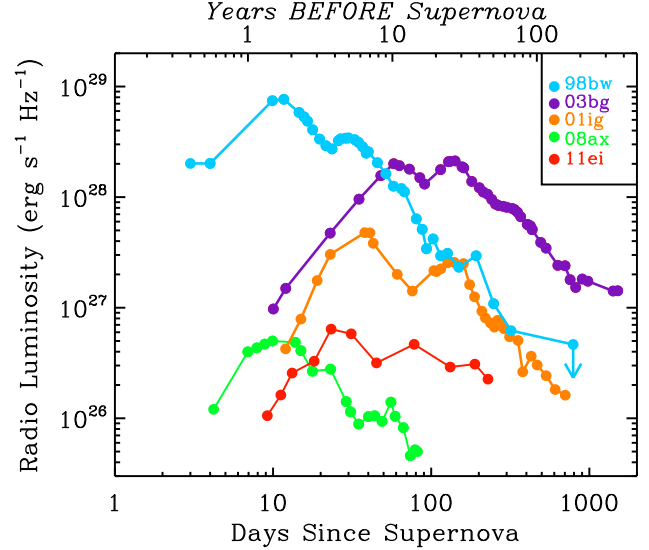


Figure 17. The 5 GHz light curve for SN 2011ei is compared to those of other radio supernovae including the Type I Ib SNe 2001ig (Ryder et al. 2004), SN 2003bg (Soderberg et al. 2006), SN 2008ax (Roming et al. 2009), and the GRB-associated Type Ic SN 1998bw (Kulkarni et al. 1998). Each of these SNe shows variable radio emission that deviates from the expected decay as roughly $F_\nu \propto t^{-1}$. In particular, all of these events show second maxima within a few months of the explosion.

5.2. Mass-loss Rate and Evidence for an Inhomogeneous Wind

Finally, we consider the mass-loss rate of the progenitor system. As shown in Figure 15, the radio light curves for SN 2011ei do not decline as a power-law following maximum light, but instead show evidence for a secondary maximum at ≈ 80 days post-outburst. As noted in Chevalier & Soderberg (2010), secondary maxima are common among SNe I Ib. Assuming the dominant absorption process is synchrotron self-absorption as suggested by Figure 16, the time averaged mass-loss rate \dot{M} from the progenitor star can be estimated as

$$\begin{aligned} \dot{M} \approx 0.38 M_\odot \text{ yr}^{-1} \\ \times (\epsilon_B/0.1)^{-1} (\epsilon_e/e_B)^{-8/19} (F_{\nu,p}/\text{mJy})^{-4/19} \\ \times (d/10 \text{ Mpc})^{-8/19} (\nu_p/5)^2 (t_p/10 \text{ days})^2, \end{aligned} \quad (5)$$

for a wind velocity of $v_w = 1000 \text{ km s}^{-1}$ typical for a WR star (Chevalier & Fransson 2006).

For reasonable values of $\epsilon_e = \epsilon_B = 0.1$ we find $\dot{M} \approx 1.4 \times 10^{-5} M_\odot \text{ yr}^{-1}$. We note that this is a

lower bound on the inferred mass-loss rate from the progenitor system. Lower values of the partition fractions and deviations from equipartition (see, e.g., SN 1993J; Fransson & Björnsson 1998) only serve to increase \dot{M} . Compared to other SNe I Ib and I bc, the mass-loss rate inferred for SN 2011ei is similar (within an order of magnitude).

As seen in Figure 17, radio light curve variations observed similar to those observed in SN 2011ei have been detected for other SNe I Ib including SN 2001ig (Ryder et al. 2004) and SN 2008ax (Roming et al. 2009), the broad-lined event SN 2003bg (Soderberg et al. 2006), as well as the GRB-associated SN 1998bw (Kulkarni et al. 1998). These fluctuations are not dissimilar in both timescale and amplitude, and have been reasonably explained in terms of density modulations in the pre-explosion environment shaped by the progenitor system (Ryder et al. 2004; Soderberg et al. 2006; Roming et al. 2009).

We adopt a model in which the radio modulations are similarly due to circumstellar density variations. As shown in Wellons et al. (2012), the optically-thin synchrotron emission scales with the number density of shocked electrons as $F_\nu \propto n_e^2$ for $p = 3$. Thus, assuming a constant compression factor by the forward shock, we find that the circumstellar density modulations scale similarly. Given the factor of ~ 3 in flux density modulations observed for SN 2011ei, we infer a factor of ~ 2 jump in the circumstellar density at a radius $r \sim 2 \times 10^{16}$ cm. Attributing this effect to a variation in the progenitor wind of the progenitor star implies an ejection timescale of $\sim 7 (v_w/10^3 \text{ km s}^{-1}) \text{ yr}$ prior to outburst.

It is intriguing to note that radio modulations have also been observed in relativistic, engine-driven SNe including GRB-SN 1998bw (Kulkarni et al. 1998; Li & Chevalier 1999) and SN 2009bb (Bietenholz et al. 2010). In these cases, the flux density modulations have been attributed to energy injection from the central engine. However, given the resemblance to the observed compact progenitor Type I Ib radio modulations, we speculate that CSM density fluctuations on radial scales of $\lesssim 10^{17}$ cm may be common among stripped-envelope SN explosions.

5.3. Limits on Inverse Compton X-ray Emission

For hydrogen-stripped SNe exploding in low density environments, the dominant X-ray emission mechanism during the first weeks to a month after the explosion is Inverse Compton (IC; Björnsson & Fransson 2004; Chevalier & Fransson 2006). In this framework, X-ray photons originate from the up-scattering of optical photons from the SN photosphere by a population of electrons accelerated to relativistic speeds by the SN shock. X-ray IC depends on the density structure of the SN ejecta, the structure of the CSM, and the details of the electron distribution responsible for the up-scattering, but does not require any assumption on magnetic field related parameters and it is not affected by possible uncertainties on the SN distance. Thus, limits on X-ray emission can provide information on the pre-SN mass-loss history of the progenitor independent of our radio analysis.

Using the reconstructed bolometric luminosity and the derived explosion parameters ($M_{ej} \sim 1.6 M_\odot$ and $E_k \sim$

2.5×10^{51} erg), and adopting the formalism discussed in Margutti et al. (2012), we estimated the progenitor mass-loss rate via X-ray IC. We assumed (i) the fraction of energy into relativistic electrons was $\epsilon_e = 0.1$ as indicated by well studied SN shocks (Chevalier & Fransson 2006), (ii) a power-law electron distribution $N(\gamma_e) = n_0 \gamma_e^{-p}$ with $p = 3$ as indicated by radio observations of SN Type I bc (Chevalier & Fransson 2006), (iii) a wind-like CSM that follows $\rho_{\text{CSM}} \propto R^{-2}$ as expected from a star which has been losing material at constant rate \dot{M} , and (iv) that the outer density structure scales as $\rho_{\text{SN}} \propto R^{-n}$ with $n \sim 10$ (see e.g., Matzner & McKee 1999; Chevalier & Fransson 2006). We find that the *Chandra* non-detection implies $\dot{M} < 2 \times 10^{-4} M_\odot \text{ yr}^{-1}$, for wind velocity $v_w = 1000 \text{ km s}^{-1}$. This calculation is consistent with the properties derived from our radio analysis (Section 5.2).

6. DISCUSSION

6.1. The Progenitor of SN 2011ei

The early onset of helium-rich features in the optical spectra of SN 2011ei and the evolution of its bolometric light curve are consistent with model explosions of He core stars with pre-supernova masses of $\sim 3 - 4 M_\odot$ (Shigeyama et al. 1990; Woosley et al. 1995). The initial presence and subsequent rapid disappearance of hydrogen suggests the progenitor star still retained a thin hydrogen envelope of mass $\sim 0.01 M_\odot$ immediately prior to outburst. In this framework, the progenitor star of SN 2011ei underwent an iron core-collapse resulting in an outburst with $E_K \sim 2.5 \times 10^{51}$ erg and ejecting some $\sim 1.6 M_\odot$ of material.

Our inferred Ni mass of $0.03 \pm 0.005 M_\odot$ for SN 2011ei is on the low end of Ni masses derived for other stripped-envelope events ($\sim 0.05 - 0.15 M_\odot$; Taubenberger et al. 2011). A low Ni mass yield is consistent with the explosions of lower-mass He star progenitors that have small iron cores ($\lesssim 0.15 M_\odot$) and eject considerably less material compared to their larger counterparts (Shigeyama et al. 1990; Hachisu et al. 1991). Lower-mass He stars are also predicted to undergo more extensive mixing compared to higher-mass stars (Hachisu et al. 1991). The helium and iron expansion velocities determined from our synthetic spectral fits to SN 2011ei are quite similar (see Figure 9), and thus are in agreement with the emitting ejecta being well-mixed.

Several properties of WR stars make them a plausible candidate progenitor for SN 2011ei: (i) WR stars are believed to be likely progenitors of at least some SNe I Ib and I bc (Heger et al. 2003), (ii) some subtypes of WR stars (e.g., the WN class) have an observable amount of hydrogen at their surface (Hamann et al. 1991), (iii) the radio-derived mass-loss rate of SN 2011ei is consistent with the observed rates for Galactic WR stars ($10^{-4} \lesssim \dot{M} \lesssim 10^{-6} M_\odot \text{ yr}^{-1}$; Hamann et al. 2006), and (iv) the radius inferred from the early photometry ($R_* \sim 1 \times 10^{11}$ cm) is consistent with those of WR stars (Crowther 2007). The putative WR star could have evolved originally from either a single star with a high main sequence mass of $\sim 25 M_\odot$, or a lower-mass star with main sequence mass $\sim 10 - 15 M_\odot$ in an interacting binary system. Metal-poor environments are associated with weaker line-driven winds (Vink & de Koter 2005),

so SN 2011ei’s slightly sub-solar metallicity suggests close binary evolution may be a more likely channel.

The physical origin of the radio light curve variations and the inferred inhomogeneous wind is not clear. Interestingly, not all radio SNe show this behavior. For instance, several well-studied examples exhibit smooth light curve evolutions, including the Type IIB SNe 1993J and 2011dh (van Dyk et al. 1994; Bartel et al. 2002; Krauss et al. 2012), and the Type Ic SN 2003L (Soderberg et al. 2005), among others. Thus, some aspect of the progenitors of stripped-envelope events like SN 2011ei (see Figure 17) produces variability in the winds of the progenitor systems on the timescale of ~ 10 yr.

Luminous blue variables (LBVs) have been suggested as possible progenitor stars given that they share many characteristics of WR stars and can undergo occasional giant eruptive events that play a major role in removing the H-rich envelope on timescales that are consistent with SN 2011ei’s radio light curve variability (see, e.g., Kotak & Vink 2006). However, SNe IIB and Ib progenitors appear to be less massive and more compact than LBVs (Soderberg et al. 2006). Ultimately, although LBVs may not represent the evolutionary state immediately prior to outburst, LBV-like eruptions may provide the dominant method of stripping the H-rich envelope at low metallicity for WR stars (Crowther 2007).

6.2. Classification Confusion: IIB vs. Ib

At the earliest epochs observed, SN 2011ei exhibited emission properties consistent with a Type II classification. However, by the time of maximum light, SN 2011ei closely resembled many SNe Ib (see Figure 11). Thus, had optical spectra of SN 2011ei been obtained less than a week later than our earliest spectrum, its early $H\alpha$ emission would have been missed and the SN likely classified as Type Ib event.

Two important lessons come from this rapid spectral evolution. One is that absorption around 6250 Å in SNe Ib can be interpreted as a clear signature of hydrogen. High-velocity hydrogen has long been suspected in SNe Ib spectra, but direct identification has been largely circumstantial because it has most often only been observed as absorption in the region of $H\alpha$. However, there are now at least two other well-observed cases where the transition of an $H\alpha$ profile showing broad emission has been monitored through to conspicuous absorption around 6250 Å: SN 2007Y (Stritzinger et al. 2009), and SN 2008ax (Chornock et al. 2011). In all cases the subsequent absorption features observed are of the same velocity and equivalent width of absorptions observed in a number of SNe Ib (see Figure 11).

The second lesson is that the rapid disappearance of $H\alpha$ emission in the early spectra of SN 2011ei underscores a classification ambiguity. Namely, *in some cases, whether an event is classified as Type Ib or IIB depends on how early the first spectrum is obtained.* Consequently, criteria that take into account the possibility of temporal selection effects should be developed to distinguish between SNe IIB and Ib. An unambiguous classification scheme is crucial if precise rates of SNe IIB vs. Ib events are to be estimated.

One possible spectral diagnostic to distinguish between

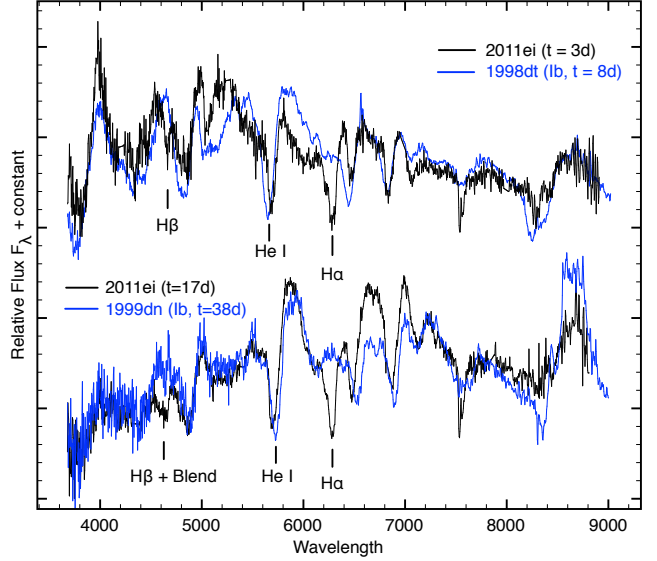


Figure 18. Spectra of SN 2011ei and the Type Ib SNe 1998dt and 1999dn (Matheson et al. 2001). The relative strength of He I $\lambda 5876$ absorption (observed near 5700 Å) to that of $H\alpha$ absorption (observed near 6250 Å) could be used as a diagnostic to distinguish between Type IIB and Ib events.

SNe IIB and Ib may be the relative strength between absorption features around 6250 and 5700 Å. In Figure 18, spectra of SN 2011ei and the Type Ib SN 1998dt (Matheson et al. 2001) obtained around the time of maximum light are plotted. Both share very similar spectral features outside of the conspicuous $H\alpha$ absorption. Also plotted in Figure 18 are later-epoch spectra of SN 2011ei and the prototypical Type Ib SN 1999dn (Matheson et al. 2001). Again, all spectral features are largely identical outside of absorptions around $H\alpha$ and $H\beta$. This pattern is observed in other SNe IIB as well; e.g., SN 1993J and SN 2001ig (see Figure 13). Thus, a Type IIB event may distinguished from a Type Ib by an $H\alpha$ absorption comparable to He I $\lambda 5876$ around the time of maximum light. This could be defined explicitly as $EW(H\alpha)/EW(\text{He I } \lambda 5876) \gtrsim 0.5$ within a few weeks of maximum.

7. CONCLUSIONS

We have presented X-ray, UV/optical, and radio observations of the He-rich, stripped-envelope, core-collapse SN 2011ei beginning within ~ 1 day of explosion. The key findings of our analyses can be summarized as follows:

1. *SN 2011ei was a relatively faint supernova with properties consistent with the outburst of a He-core star that suffered modest episodic mass-loss.* We suggest that a $3 - 4 M_{\odot}$ WR star of radius $R_{*} \sim 1 \times 10^{11}$ cm that retained a thin hydrogen envelope immediately prior to outburst is a plausible candidate progenitor for SN 2011ei. The explosion had an energy $E_K \sim 2.5 \times 10^{51}$ erg, ejected some $\sim 1.6 M_{\odot}$ of material, and had a peak bolometric luminosity of $L_{bol} \sim 7 \times 10^{41}$ ergs $^{-1}$. Radio light curve fluctuations in SN 2011ei suggest quasi-periodic mass-loss episodes prior to outburst. These inhomogeneities are similar to a subset of

other radio SNe and complicate the standard picture for smooth radiation-driven stellar winds.

2. *High-velocity hydrogen is not rare in SNe Ib.* Identification of hydrogen in Type Ib spectra has been largely circumstantial because it has most often only been observed as absorption around $H\alpha$. In SN 2011ei, however, the transition of hydrogen emission through to absorption was closely monitored to identify its origin unambiguously. This evolution supports notions of a spectroscopic sequence bridging SNe I Ib, SNe Ib that have deep $H\alpha$ absorptions, and typical SNe Ib via a common progenitor scenario potentially rooted in differences in the hydrogen envelope mass. Whether this has origins in binary interaction and/or strong stellar winds is not clear, but circumstantial evidence suggests stellar duplicity plays a role in at least some cases.
3. *Time-dependent classifications of SNe I Ib and Ib bias estimates of their explosion rates.* Like SN 2007Y (Stritzinger et al. 2009) and SN 2008ax (Chornock et al. 2011), SN 2011ei was caught early enough to observe a rapid evolution from Type II to Type Ib features in its pre-maximum light spectra. While SNe I Ib have traditionally been understood to undergo this transformation on the timescale of months, examples such as SN 2011ei establish that the metamorphosis can occur on the timescale of a few days. Consequently, how close an observation is made relative to the time of explosion is a significant factor in a Type I Ib vs. Ib classification, and this has implications in determining precise rates.

Study of SN 2011ei shows that defining SNe Ib solely on the absence of hydrogen can lead to a classification confusion. There is no clear separation of SNe I Ib vs. Ib for at least a subset of these events. Instead, it is a gradual transition depending on remaining hydrogen mass. Along similar lines, the current definition of SNe Ic as lacking both hydrogen and helium lines may require revision. It is common practice to model SNe Ic in terms of core-collapse in bare carbon-oxygen cores (Iwamoto et al. 1994; Foley et al. 2003; Mazzali et al. 2004). However, there have been many reports of hydrogen and helium in SNe Ic (Filippenko 1988, 1992; Filippenko et al. 1990; Jeffery et al. 1991; Branch et al. 2002, 2006), and many objects exhibit properties that bridge SNe Ib and Ic subtypes; e.g., SN 2008D (Soderberg et al. 2008), and SN 2009jf (Valenti et al. 2011).

Thus, similar temporal selection effects may be at the root of uncertain line identifications in SNe Ib and Ic. We recommend that multi-wavelength data suites like the one presented here could help resolve these ambiguities. Investigations of new SNe Ibc should incorporate high-cadence (~ 2 day) spectroscopic and photometric monitoring in the UV/optical commencing within days of explosion, and be coordinated with follow-up X-ray and radio observations. From these panchromatic data, unique information about the progenitor star's poorly understood evolutionary state and associated mass-loss in the days to years prior to SN outburst can be extracted. Accumulation of even just a handful of addi-

tional objects studied in this way could establish fresh new insights into the nature of stripped-envelope SN explosions.

We thank R. Chornock for helpful comments that improved the manuscript. Some of the observations reported in this paper were obtained with the Southern African Large Telescope (SALT), as well as the 6.5 meter Magellan Telescopes located at Las Campanas Observatory, Chile. Additional observations were obtained at the Southern Astrophysical Research (SOAR) telescope, which is a joint project of the Ministério da Ciência, Tecnologia, e Inovação (MCTI) da República Federativa do Brasil, the U.S. National Optical Astronomy Observatory (NOAO), the University of North Carolina at Chapel Hill (UNC), and Michigan State University (MSU). Support for this work was provided by the National Aeronautics and Space Administration through Chandra Award Number 12500613 issued by the Chandra X-ray Observatory Center, which is operated by the Smithsonian Astrophysical Observatory for and on behalf of the National Aeronautics Space Administration under contract NAS8-03060. The National Radio Astronomy Observatory is a facility of the National Science Foundation operated under cooperative agreement by Associated Universities, Inc. L. C. is a Jansky Fellow of the National Radio Astronomy Observatory. G. P. acknowledges support from “proyecto regular UNAB” DI-28-11/R. All SAAO and SALT co-authors acknowledge the support from the National Research Foundation (NRF) of South Africa. A. B. was supported by a Marie Curie Outgoing International Fellowship (FP7) of the European Union (project number 275596). G. P., F. B., and J. A. acknowledge support provided by the Millennium Center for Supernova Science through grant P10-064-F (funded by “Programa Bicentenario de Ciencia y Tecnología de CONICYT” and “Programa Iniciativa Científica Milenio de MIDEPLAN”). J. A. acknowledges support by CONICYT through FONDECYT grant 3110142, and by the Millennium Center for Supernova Science (P10-064-F), with input from the “Fondo de Innovación para La Competitividad, de Ministerio de Economía, Fomento Y Turismo de Chile.” Partially based on observations (program ID 184.D-1140) collected at the European Organisation for Astronomical Research in the Southern Hemisphere, Chile. S. B. is partially supported by the PRIN-INAF 2009 with the project “Supernovae Variety and Nucleosynthesis Yields.” This paper made extensive use of the SUSPECT database (<http://www.nhn.ou.edu/suspect/>). IRAF is distributed by the National Optical Astronomy Observatory, which is operated by the Association of Universities for Research in Astronomy (AURA) under cooperative agreement with the National Science Foundation. PYRAF is a product of the Space Telescope Science Institute, which is operated by AURA for NASA. Dust maps were accessed via the NASA/IPAC Infrared Science archive at <http://irsa.ipac.caltech.edu/applications/DUST/>.

Facilities: SALT (RSS), Magellan:Baade (IMACS), Magellan:Clay (LDSS3) SWIFT (UVOT,XRT), CXO, SOAR (Goodman), NTT (EFOSC2), CTIO: PROMPT

REFERENCES

- Anderson, J. P., Covarrubias, R. A., James, P. A., Hamuy, M., & Haberman, S. M. 2010, *MNRAS*, 407, 2660
- Anupama, G. C., Sahu, D. K., Deng, J., et al. 2005, *ApJ*, 631, L125
- Arcavi, I., Gal-Yam, A., Kasliwal, M. M., et al. 2010, *ApJ*, 721, 777
- Arcavi, I., Gal-Yam, A., Yaron, O., et al. 2011, *ApJ*, 742, L18
- Asplund, M., Grevesse, N., & Sauval, A. J. 2005, in *Astronomical Society of the Pacific Conference Series*, Vol. 336, *Cosmic Abundances as Records of Stellar Evolution and Nucleosynthesis*, ed. T. G. Barnes III & F. N. Bash, 25
- Baron, E., Hauschildt, P. H., & Branch, D. 1994, *ApJ*, 426, 334
- Baron, E., Hauschildt, P. H., Branch, D., et al. 1995, *ApJ*, 441, 170
- Bartel, N., Bietenholz, M. F., Rupen, M. P., et al. 2002, *ApJ*, 581, 404
- Bartunov, O. S., Blinnikov, S. I., Pavlyuk, N. N., & Tsvetkov, D. Y. 1994, *A&A*, 281, L53
- Benetti, S., Branch, D., Turatto, M., et al. 2002, *MNRAS*, 336, 91
- Benetti, S., Turatto, M., Valenti, S., et al. 2011, *MNRAS*, 411, 2726
- Bietenholz, M. F., Soderberg, A. M., Bartel, N., et al. 2010, *ApJ*, 725, 4
- Bietenholz, M. F., Bartel, N., Rupen, M. P., et al. 2011, *ArXiv e-prints*, [arXiv:1103.1783](https://arxiv.org/abs/1103.1783) [[astro-ph.CO](https://arxiv.org/abs/1103.1783)]
- Bigelow, B. C., Dressler, A. M., Shectman, S. A., & Epps, H. W. 1998, in *Society of Photo-Optical Instrumentation Engineers (SPIE) Conference Series*, Vol. 3355, *Society of Photo-Optical Instrumentation Engineers (SPIE) Conference Series*, ed. S. D'Odorico, 225
- Björnsson, C.-I., & Fransson, C. 2004, *ApJ*, 605, 823
- Branch, D. 1972, *A&A*, 16, 247
- Branch, D., Jeffery, D. J., Young, T. R., & Baron, E. 2006, *PASP*, 118, 791
- Branch, D., Benetti, S., Kasen, D., et al. 2002, *ApJ*, 566, 1005
- Brown, P. J., Holland, S. T., Immler, S., et al. 2009, *AJ*, 137, 4517
- Burgh, E. B., Nordsieck, K. H., Kobulnicky, H. A., et al. 2003, in *Presented at the Society of Photo-Optical Instrumentation Engineers (SPIE) Conference*, Vol. 4841, *Society of Photo-Optical Instrumentation Engineers (SPIE) Conference Series*, ed. M. Iye & A. F. M. Moorwood, 1463
- Burrows, D. N., Hill, J. E., Nousek, J. A., et al. 2005, *Space Sci. Rev.*, 120, 165
- Cappellaro, E., Mazzali, P. A., Benetti, S., et al. 1997, *A&A*, 328, 203
- Chevalier, R. A. 1982, *ApJ*, 259, 302
- Chevalier, R. A. 1998, *ApJ*, 499, 810
- Chevalier, R. A., & Fransson, C. 2006, *ApJ*, 651, 381
- Chevalier, R. A., & Fransson, C. 2008, *ApJ*, 683, L135
- Chevalier, R. A., & Soderberg, A. M. 2010, *ApJ*, 711, L40
- Chomiuk, L., & Soderberg, A. 2011, *The Astronomer's Telegram*, 3532, 1
- Chornock, R., Filippenko, A. V., Li, W., et al. 2011, *ApJ*, 739, 41
- Chugai, N. N. 2000, *Astronomy Letters*, 26, 797
- Clemens, J. C., Crain, J. A., & Anderson, R. 2004, in *Society of Photo-Optical Instrumentation Engineers (SPIE) Conference Series*, Vol. 5492, *Society of Photo-Optical Instrumentation Engineers (SPIE) Conference Series*, ed. A. F. M. Moorwood & M. Iye, 331
- Clocchiatti, A., Wheeler, J. C., Phillips, M. M., et al. 1997, *ApJ*, 483, 675
- Crawford, S. M., Still, M., Schellart, P., et al. 2010, in *Society of Photo-Optical Instrumentation Engineers (SPIE) Conference Series*, Vol. 7737, *Society of Photo-Optical Instrumentation Engineers (SPIE) Conference Series*
- Crockett, R. M., Eldridge, J. J., Smartt, S. J., et al. 2008, *MNRAS*, 391, L5
- Crowther, P. A. 2007, *ARA&A*, 45, 177
- Deng, J. S., Qiu, Y. L., Hu, J. Y., Hatano, K., & Branch, D. 2000, *ApJ*, 540, 452
- Dessart, L., Hillier, D. J., Livne, E., et al. 2011, *MNRAS*, 414, 2985
- Drout, M. R., Soderberg, A. M., Gal-Yam, A., et al. 2011, *ApJ*, 741, 97
- Eldridge, J. J., Izzard, R. G., & Tout, C. A. 2008, *MNRAS*, 384, 1109
- Ensmann, L., & Burrows, A. 1992, *ApJ*, 393, 742
- Filippenko, A. V. 1988, *AJ*, 96, 1941
- Filippenko, A. V. 1992, *ApJ*, 384, L37
- Filippenko, A. V. 1997, *ARA&A*, 35, 309
- Filippenko, A. V., Matheson, T., & Barth, A. J. 1994, *AJ*, 108, 2220
- Filippenko, A. V., Matheson, T., & Ho, L. C. 1993, *ApJ*, 415, L103
- Filippenko, A. V., Porter, A. C., & Sargent, W. L. W. 1990, *AJ*, 100, 1575
- Folatelli, G., Contreras, C., Phillips, M. M., et al. 2006, *ApJ*, 641, 1039
- Foley, R. J., Sanders, N. E., & Kirshner, R. P. 2011, *ApJ*, 742, 89
- Foley, R. J., Papenkova, M. S., Swift, B. J., et al. 2003, *PASP*, 115, 1220
- Foley, R. J., Challis, P. J., Filippenko, A. V., et al. 2012, *ApJ*, 744, 38
- Fransson, C., & Björnsson, C.-I. 1998, *ApJ*, 509, 861
- Fryer, C. L., Mazzali, P. A., Prochaska, J., et al. 2007, *PASP*, 119, 1211
- Gehrels, N., Chincarini, G., Giommi, P., et al. 2004, *ApJ*, 611, 1005
- Georgy, C. 2012, *A&A*, 538, L8
- Hachinger, S., Mazzali, P. A., Taubenberger, S., et al. 2012, *MNRAS*, 422, 70
- Hachisu, I., Matsuda, T., Nomoto, K., & Shigeyama, T. 1991, *ApJ*, 368, L27
- Hamann, W.-R., Duennebeil, G., Koesterke, L., Wessolowski, U., & Schmutz, W. 1991, *A&A*, 249, 443
- Hamann, W.-R., Gräfener, G., & Liermann, A. 2006, *A&A*, 457, 1015
- Hamuy, M., Suntzeff, N. B., Heathcote, S. R., et al. 1994, *PASP*, 106, 566
- Hamuy, M., Walker, A. R., Suntzeff, N. B., et al. 1992, *PASP*, 104, 533
- Hamuy, M., Maza, J., Pinto, P. A., et al. 2002, *AJ*, 124, 417
- Hamuy, M., Deng, J., Mazzali, P. A., et al. 2009, *ApJ*, 703, 1612
- Harkness, R. P., Wheeler, J. C., Margon, B., et al. 1987, *ApJ*, 317, 355
- Heger, A., Fryer, C. L., Woosley, S. E., Langer, N., & Hartmann, D. H. 2003, *ApJ*, 591, 288
- Houck, J. C., & Fransson, C. 1996, *ApJ*, 456, 811
- Iwamoto, K., Nomoto, K., Hoflich, P., et al. 1994, *ApJ*, 437, L115
- James, S., & Baron, E. 2010, *ApJ*, 718, 957
- Jeffery, D. J., Branch, D., Filippenko, A. V., & Nomoto, K. 1991, *ApJ*, 377, L89
- Jeffery, D. J., Ketchum, W., Branch, D., et al. 2007, *ApJS*, 171, 493
- Kalberla, P. M. W., Burton, W. B., Hartmann, D., et al. 2005, *A&A*, 440, 775
- Kelly, P. L., & Kirshner, R. P. 2011, *ArXiv e-prints*, [arXiv:1110.1377](https://arxiv.org/abs/1110.1377) [[astro-ph.CO](https://arxiv.org/abs/1110.1377)]
- Kewley, L. J., & Ellison, S. L. 2008, *ApJ*, 681, 1183
- Koribalski, B. S., Staveley-Smith, L., Kilborn, V. A., et al. 2004, *AJ*, 128, 16
- Kotak, R., & Vink, J. S. 2006, *A&A*, 460, L5
- Krauss, M. I., Soderberg, A. M., Chomiuk, L., et al. 2012, *ArXiv e-prints*, [arXiv:1201.0770](https://arxiv.org/abs/1201.0770) [[astro-ph.HE](https://arxiv.org/abs/1201.0770)]
- Kulkarni, S. R., Frail, D. A., Wieringa, M. H., et al. 1998, *Nature*, 395, 663
- Landolt, A. U. 1992, *AJ*, 104, 340
- Landolt, A. U. 2007, *AJ*, 133, 2502
- Lewis, J. R., Walton, N. A., Meikle, W. P. S., et al. 1994, *MNRAS*, 266, L27
- Li, W., Leaman, J., Chornock, R., et al. 2011, *MNRAS*, 412, 1441
- Li, Z.-Y., & Chevalier, R. A. 1999, *ApJ*, 526, 716
- Maeda, K., Kawabata, K., Mazzali, P. A., et al. 2008, *Science*, 319, 1220
- Margutti, R., Soderberg, A. M., Chomiuk, L., et al. 2012, *ApJ*, 751, 134
- Martí-Vidal, I., Marcaide, J. M., Alberdi, A., et al. 2011, *A&A*, 526, A142
- Matheson, T., Filippenko, A. V., Li, W., Leonard, D. C., & Shields, J. C. 2001, *AJ*, 121, 1648

- Matheson, T., Filippenko, A. V., Barth, A. J., et al. 2000, *AJ*, 120, 1487
- Matzner, C. D., & McKee, C. F. 1999, *ApJ*, 510, 379
- Maund, J. R., Smartt, S. J., Kudritzki, R. P., Podsiadlowski, P., & Gilmore, G. F. 2004, *Nature*, 427, 129
- Maund, J. R., Fraser, M., Ergon, M., et al. 2011, *ApJ*, 739, L37
- Maurer, I., Mazzali, P. A., Taubenberger, S., & Hachinger, S. 2010, *MNRAS*, 409, 1441
- Mazzali, P. A., Deng, J., Hamuy, M., & Nomoto, K. 2009, *ApJ*, 703, 1624
- Mazzali, P. A., Deng, J., Maeda, K., et al. 2004, *ApJ*, 614, 858
- Mazzali, P. A., Kawabata, K. S., Maeda, K., et al. 2005, *Science*, 308, 1284
- Mazzali, P. A., Valenti, S., Della Valle, M., et al. 2008, *Science*, 321, 1185
- Milisavljevic, D., Fesen, R. A., Gerardy, C. L., Kirshner, R. P., & Challis, P. 2010, *ApJ*, 709, 1343
- Milisavljevic, D., Fesen, R., Nordsieck, K., et al. 2011, *The Astronomer's Telegram*, 3526, 1
- Modjaz, M., Kewley, L., Bloom, J. S., et al. 2011, *ApJ*, 731, L4
- Modjaz, M., Kirshner, R. P., Blondin, S., Challis, P., & Matheson, T. 2008, *ApJ*, 687, L9
- Modjaz, M., Li, W., Butler, N., et al. 2009, *ApJ*, 702, 226
- Murphy, J. W., Jennings, Z. G., Williams, B., Dalcanton, J. J., & Dolphin, A. E. 2011, *ApJ*, 742, L4
- Nakar, E., & Sari, R. 2010, *ApJ*, 725, 904
- Nomoto, K. I., Iwamoto, K., & Suzuki, T. 1995, *Phys. Rep.*, 256, 173
- Oke, J. B. 1990, *AJ*, 99, 1621
- Parrent, J., Branch, D., Troxel, M. A., et al. 2007, *PASP*, 119, 135
- Pastorello, A., Kasliwal, M. M., Crockett, R. M., et al. 2008, *MNRAS*, 389, 955
- Perley, R. A., Chandler, C. J., Butler, B. J., & Wrobel, J. M. 2011, *ApJ*, 739, L1
- Pettini, M., & Pagel, B. E. J. 2004, *MNRAS*, 348, L59
- Podsiadlowski, P., Joss, P. C., & Hsu, J. J. L. 1992, *ApJ*, 391, 246
- Poole, T. S., Breeveld, A. A., Page, M. J., et al. 2008, *MNRAS*, 383, 627
- Poznanski, D., Ganeshalingam, M., Silverman, J. M., & Filippenko, A. V. 2011, *MNRAS*, 415, L81
- Predehl, P., & Schmitt, J. H. M. M. 1995, *A&A*, 293, 889
- Prieto, J. L., Stanek, K. Z., & Beacom, J. F. 2008, *ApJ*, 673, 999
- Puls, J., Vink, J. S., & Najarro, F. 2008, *A&A Rev.*, 16, 209
- Qiu, Y., Li, W., Qiao, Q., & Hu, J. 1999, *AJ*, 117, 736
- Reichart, D., Nysewander, M., Moran, J., et al. 2005, *Nuovo Cimento C Geophysics Space Physics C*, 28, 767
- Richardson, D., Branch, D., & Baron, E. 2006, *AJ*, 131, 2233
- Richmond, M. W., Treffers, R. R., Filippenko, A. V., et al. 1994, *AJ*, 107, 1022
- Roming, P. W. A., Kennedy, T. E., Mason, K. O., et al. 2005, *Space Sci. Rev.*, 120, 95
- Roming, P. W. A., Pritchard, T. A., Brown, P. J., et al. 2009, *ApJ*, 704, L118
- Ryder, S. D., Sadler, E. M., Subrahmanyam, R., et al. 2004, *MNRAS*, 349, 1093
- Sanders, N. E., Soderberg, A. M., Levesque, E. M., et al. 2012, *ArXiv e-prints*, [arXiv:1206.2643 \[astro-ph.HE\]](#)
- Schlegel, D. J., Finkbeiner, D. P., & Davis, M. 1998, *ApJ*, 500, 525
- Shigeyama, T., Nomoto, K., Tsujimoto, T., & Hashimoto, M.-A. 1990, *ApJ*, 361, L23
- Shigeyama, T., Suzuki, T., Kumagai, S., et al. 1994, *ApJ*, 420, 341
- Silverman, J. M., Mazzali, P., Chornock, R., et al. 2009, *PASP*, 121, 689
- Smartt, S. J. 2009, *ARA&A*, 47, 63
- Smith, N., Li, W., Filippenko, A. V., & Chornock, R. 2011, *MNRAS*, 412, 1522
- Smith, N., & Owocki, S. P. 2006, *ApJ*, 645, L45
- Soderberg, A. M., Chevalier, R. A., Kulkarni, S. R., & Frail, D. A. 2006, *ApJ*, 651, 1005
- Soderberg, A. M., Kulkarni, S. R., Berger, E., et al. 2005, *ApJ*, 621, 908
- Soderberg, A. M., Berger, E., Page, K. L., et al. 2008, *Nature*, 453, 469
- Soderberg, A. M., Margutti, R., Zauderer, B. A., et al. 2011, *ArXiv e-prints*, [arXiv:1107.1876 \[astro-ph.HE\]](#)
- Springob, C. M., Masters, K. L., Haynes, M. P., Giovanelli, R., & Marinoni, C. 2009, *ApJS*, 182, 474
- Stritzinger, M., Hamuy, M., Suntzeff, N. B., et al. 2002, *AJ*, 124, 2100
- Stritzinger, M., Mazzali, P., Phillips, M. M., et al. 2009, *ApJ*, 696, 713
- Stritzinger, M., Morrell, N., Pignata, G., et al. 2011, *Central Bureau Electronic Telegrams*, 2777, 1
- Sutherland, P. G., & Wheeler, J. C. 1984, *ApJ*, 280, 282
- Tanaka, M., Yamanaka, M., Maeda, K., et al. 2009, *ApJ*, 700, 1680
- Taubenberger, S., Valenti, S., Benetti, S., et al. 2009, *MNRAS*, 397, 677
- Taubenberger, S., Navasardyan, H., Maurer, J. I., et al. 2011, *MNRAS*, 413, 2140
- Thomas, R. C., Nugent, P. E., & Meza, J. C. 2011, *PASP*, 123, 237
- Turatto, M., Benetti, S., & Cappellaro, E. 2003, in *From Twilight to Highlight: The Physics of Supernovae*, ed. W. Hillebrandt & B. Leibundgut, 200
- Valenti, S., Benetti, S., Cappellaro, E., et al. 2008, *MNRAS*, 383, 1485
- Valenti, S., Fraser, M., Benetti, S., et al. 2011, *MNRAS*, 416, 3138
- van Dyk, S. D., Weiler, K. W., Sramek, R. A., Rupen, M. P., & Panagia, N. 1994, *ApJ*, 432, L115
- Van Dyk, S. D., Li, W., Cenko, S. B., et al. 2011, *ApJ*, 741, L28
- Vink, J. S., & de Koter, A. 2005, *A&A*, 442, 587
- Watson, D. 2011, *A&A*, 533, A16
- Wellons, S., Soderberg, A. M., & Chevalier, R. A. 2012, *ArXiv e-prints*, [arXiv:1201.5120 \[astro-ph.HE\]](#)
- Willeck, J. A., Courteau, S., Faber, S. M., et al. 1997, *ApJS*, 109, 333
- Woosley, S. E., Eastman, R. G., Weaver, T. A., & Pinto, P. A. 1994, *ApJ*, 429, 300
- Woosley, S. E., Langer, N., & Weaver, T. A. 1995, *ApJ*, 448, 315
- Yoon, S.-C., Woosley, S. E., & Langer, N. 2010, *ApJ*, 725, 940
- Zhang, Q., Hu, J. Y., Wang, L. F., Mazzali, P. A., & Wang, Z. R. 1995a, *MNRAS*, 277, 1115
- Zhang, Q., Wang, L., Hu, J., Mazzali, P. A., & Wang, Z. 1995b, *Acta Astrophysica Sinica*, 15, 228
- Zhang, Q., & Wang, Z. R. 1996, *A&A*, 307, 166